Stony Brook University

High Performance Two-Phase Thermosyphon for Energy-Efficient Refrigeration Applications: Modeling and Experiments

A Thesis Presented

by

Chunlei Mei

to

The Graduate School

in Partial Fulfillment of the

Requirements

for the Degree of

Master of Science

in

Mechanical Engineering

Stony Brook University

May 9th 2013

Stony Brook University

The Graduate School

Chunlei Mei

We, the thesis committee for the above candidate for the

Master of Science degree, hereby recommend

acceptance of this thesis.

Jon Longtin – Thesis Advisor
Professor, Mechanical Engineering Department

David Hwang – Second Reader
Professor, Mechanical Engineering Department

John Kincaid – Chairperson of Defense
Professor, Mechanical Engineering Department

This thesis is accepted by the Graduate School

Charles Taber
Interim Dean of the Graduate School

Abstract of the Thesis

High Performance Two-Phase Thermosyphon for Energy-Efficient Refrigeration Applications: Modeling and Experiments

by

Chunlei Mei

Master of Science

in

Mechanical Engineering

Stony Brook University

2013

The Two-Phase Closed Thermosyphon (TPCT) is a device that transfers heat from its bottom to top and because phase change phenomenon happens both in its bottom and top, its performance is ten times better than pure metal. It has three heat transfer regimes, condenser, adiabatic section and evaporator. The mechanism of thermosyphon is the phase change cycle: liquid absorbs heat in evaporator and then vaporizes into vapor; finally the vapor condenses along the condenser wall and flow back to evaporator liquid pool.

Firstly, detailed heat transfer mechanism will be discussed. Many empirical equations will be reviewed. Geometrically, TPCT contains three parts, condenser, adiabatic section and evaporator, and each of them has three possible mechanism, natural convection, nucleate boiling and transit convection between these two. In evaporator, it contains both film and pool area. Thus, comprehensively heat transfer mechanism literature review is needed and it is the preparation for building model.

A numerical model is built from basic governing equations and empirical equations. It is suitable for any kind of liquids and covers wide range of geometry size and power input. With this model, important TPCT parameters, such as filling ratio, power input, pipe diameter, and so on, are researched theoretically.

An experiment system is built up. Through this, power input and working fluids filling ratio are controlled based on need. Temperature along outer pipe wall and vapor pressure are collected by this system. Lots of experiment data about methanol and ethanol are listed in figures and charts. Comparison between simulation and experiment is conducted.

Creatively, new fluids are applied in this project. Experiment data about aluminum oxide nanofluids, ethanol-water azeotrope and ethanol-methanol mixture are listed.

Table of Contents

List of Figures

List of Tables

Nomenclature

Ar	Archimid number
Bo	Bond number based on inner diameter
c_p	Heat capacity $[J\ kg^{-1}K^{-1}]$
C_{sf}	Coefficient
C_f	Frictional coefficient
d, D	Diameter $[m]$
f	Friction factor
Fr	Froude number
g	Local gravity constant $[m\ s^{-2}]$
h	Heat transfer coefficient $[W\ m^{-2}K^{-1}]$
h_{fg}	Latent heat $[J\ kg^{-1}]$
h_{ku}	Kutatelatze's nucleate boiling heat transfer coefficient $[W\ m^{-2}K^{-1}]$
I_m	Scale length
K_p	Dimensionless parameter
L	Length $[m]$
M	Mass $[kg]$; molecular weight $[kg\ \ mole^{-1}]$
Nu	Nusselt number
$N_{\mu f}$	Viscosity number,
p,P	Pressure $[Pa]$
P_a	Atmosphere pressure $[Pa]$
p_c	Critical pressure $[Pa]$
p_r	Reduced pressure $[Pa]$
Pr	Prandtl number
q	Heat flux$[W\ m^{-2}]$
Q	Total amount of heat transfer $[W]$
R	Radius of thermosyphon $[m]$
Ra	Rayleigh number
Re	Reynolds number
Re_{lv}	Vapor-liquid relative velocity Reynolds number

T	Temperature [℃]
u	Velocity $[m\ s^{-1}]$
v	Velocity $[m\ s^{-1}]$
V_{vj}	Drift velocity
X	Dimensionless parameter

Greek symbols

α	Void fraction
β	Thermal expansion $[K^{-1}]$
ξ	Initial filling $[\frac{L_{filling}}{L_e}]$
ρ	Density $[kg\ m^{-3}]$
λ	Thermal conductivity $[W\ m^{-1}K^{-1}]$
η	Dimensionless parameter
μ	Dynamic viscosity $[Pa\ m]$
Φ	Power throughput $[W]$
φ	Volume concentration
δ	Thickness $[m]$
σ	Surface tension $[N\ m^{-1}]$
τ	Shear stress $[N\ m^{-2}]$
ν	Kinematic viscosity $[m^2\ s^{-1}]$
Ψ	Dimensionless parameter

Subscripts

a	Adiabatic section
c	Condenser
CC	Combined convection
e	Evaporator
ef	Film area in evaporator
eff	Effective value
exit	Exit
f	Film, friction
g	Gas

i	Inner surface, L-V interface, initial
Ku	Kutatelatze
l	Liquid
m	Momentum, average
NB	Nucleate boiling
NC	Natural convection
p	Liquid pool in evaporator
s	Saturate status
TC	Two-phase Convection
TS	Thermosyphon
v	Vapor
w	Wall
wc	Condenser wall
z	Local

Superscripts

$*$	Dimensionless
$+$	Dimensionless

Abbreviations

CCFL	Counter Current Flooding Limit
EFL	Evaporator Flooding Limit
FOM	Figure of Merit
LFDL	Liquid Film Dryout Limit
LSL	Liquid Starvation Limit
TPCT	Two-Phase Closed Thermosyphon

Acknowledgments

First, I want to say thanks to my advisor Prof. Longtin. Nearly two years has gone, since October 2011. Prof. Longtin always gives me guide and help both in my academic field and my life. I will be successful in the future because I am now standing on his shoulder.

I would like to express my appreciation to my lab mates and roommate. Two year in Stony Brook University, they help me a lot and my memory in U.S. are all with them. Tao He is my partner in this project. I can't finish this project without his help.

Also, I am grateful to the members of my thesis committees, Prof. Hwang, and Prof. Kincaid, for their valuable advice and comments.

Last and the most important is my acknowledgement to my parents. Their endless love and support let me being strong and brave. It is them who motive me going forward. I can realize my dream because they always stand behind me. Thanks.

Chapter 1

Introduction

1.1 Introduction and Application

The Two-Phase Closed Thermosyphon (TPCT) is a device that transfers heat from its bottom to top and because phase change phenomenon happens both in its bottom and top, its performance is ten times better than pure metal.

A typical TPCT is shown in Fig 1.1. It has three heat transfer regimes, condenser, adiabatic section and evaporator. According to its application, each section has relative different length. In Chapter 3, the effects of each length will be discussed in details. The mechanism of thermosyphon is the phase change cycle: liquid-vapor-liquid. The vapor generated in evaporator is the sum of two parts: (a) liquid film, which extends from the adiabatic section exit to the liquid pool surface and (b) liquid pool, in the lower portion of evaporator. Then vapor goes up and condenses along the inner pipe wall in condenser. Then heat is given away by the cooling process, usually convective heat transfer, outside the condenser; in this research, we use water cooling jacket. After that because of gravity, the condensation liquid forms the liquid film and falls back to pool along the pipe wall. Although adiabatic section is not involved in heat transfer process, it is an essential part in application. In adiabatic section, the liquid film keeps constant thickness so we can adjust its length to fit for different application conditions.

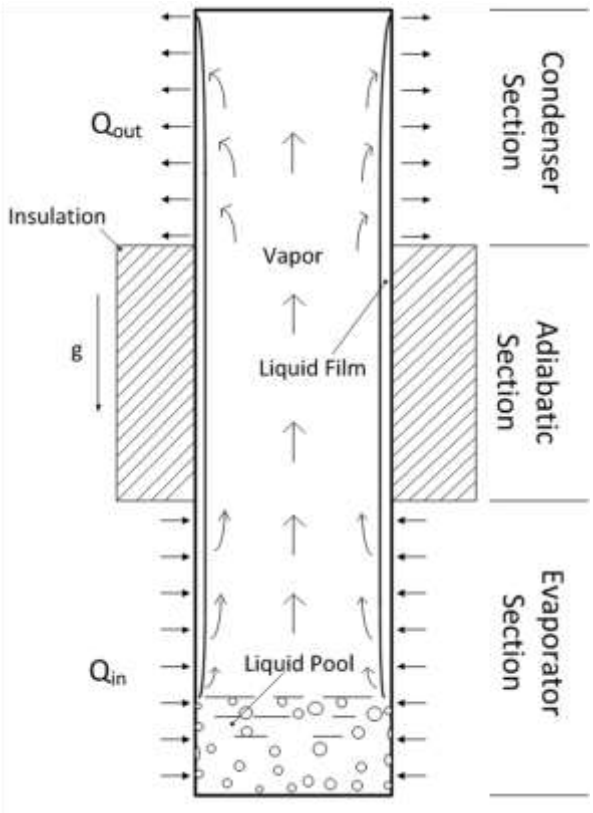

Figure 1.1 A schematic of typical thermosyphon

One feature of TPCT is called “thermal diode”, showing in fig. 1.2. It means heat transfer orientation is only possible from bottom to top. If the environment temperature of condenser is higher than that of evaporator, as condenser lacks of working liquids, no evaporation will happen and heat can only transferred by conduction along pipe wall, which is negligible.

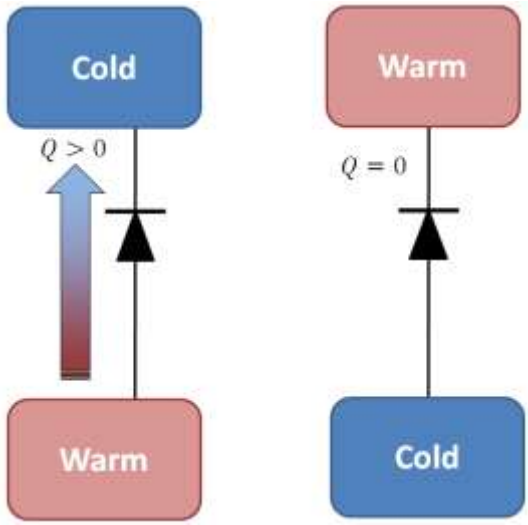

Figure 1.2 Thermosyphon works as thermal diode

Because of its high efficiency, low cost, simple to maintenance, thermosyphon is widely used in area where non-contact heat exchange is needed and place where heat sink and heat source has some distance. In power plant, thermosyphon applies the "waste heat" in exhaust to preheat the air to boiler. In building energy field, thermosyphon can also save energy from exhaust.

One thing needs to know is that thermosyphon is different from heat pipe, which has wick in its inner wall.

1.2 Basic Concept

There are many parameters describing the operation and performance of thermosyphon. The first one is filling ratio, ξ. It equals to the ratio of initial pool length (at zero power throughput) to evaporator length,

$$\xi = \frac{L_{filling}}{L_e} \tag{1-1}$$

During operation, the liquid pool height initially decreases due to formation of liquid film. Then with more power input, boiling happens in liquid pool, causing void fraction in pool because of bubbles. High temperature leads to liquid thermal expansion as well. Finally the pool height would go over the initial value. Too much filling will reduce the thermosyphon performance, as the thermal resistance in film area is ten times lower than pool area; while too less filling will cause heat transfer limits, which are discussed in chapter 2.3.

The inclination θ indicates the angle between thermosyphon and ground. Researchers [1-4] has done many experiments to discover the relationship between inclination and performance. These data cover angles from 10° to 90° including water, R-113, Methanol and other working liquids. In this research, the inclination is constant, 90°.

The choice of working liquids directly affects TPCT's performance. Figure of Merit (FOM) is used to predict the performance of liquids,

$$FOM = \left(\frac{h_{fg}\lambda_l^3\rho_l^2}{\mu_l}\right)^{0.25} \tag{1-2}$$

For common liquids, their thermal conductivity is much lower than metal, usually less than 0.6 W/(m*K). On the other hand, heat conduction is the dominant process for heat penetrates liquid film in condenser and evaporator. And also thermal conductivity is related to convective heat transfer in liquid pool. So 0.1 W/(m*K) conductivity difference among liquids will make much performance enhancement. Heat of vaporization is essential as it indicates the amount of phase change heat per unit mass. Viscosity has negative effect on performance as it will reduce the heat transfer in liquid film.

Table 1. 1 Table of FOM for common liquids

Name	ammonia	water	methanol	R32	dimethylether	acetone	R41	ethanol
FOM	4719	4177	1750	1600	1525	1455	1382	1162

There are two types of boundary conditions in evaporator, constant temperature and constant heat flux. In most literatures both in simulation and experimental, the operation condition is constant heat flux, including this one.

As mentioned above, there are three sections in thermosyphon: condenser, adiabatic section and evaporator. In evaporator, it has both liquid film and liquid pool. For the liquid film in evaporator and condenser, they have different mechanism because one is evaporation and another is condensation. In film region, it has three heat transfer types: laminar flow, combined convection and turbulence flow. However in liquid pool it has another three different heat transfer mechanisms: natural convection, combined convection and nucleate boiling. These difference make the thermosyphon analysis complex.

1.3 Research Objective

Literatures have researched thermosyphon in every aspect. This study is not just only literature reviews, but also shows the new simulation model and new experiment results. The objectives are listed as below:

(a) Build up the analytical model for the whole thermosyphon. According to chapter 1.2, the heat transfer mechanisms are so complicated that some of them only have empirical equations. This model should include and determine all these mechanisms.

(b) In simulation, different power input, filling ratio, geometry parameters as well as fluids will be studied. The purpose is to find the right fluids at reasonable filling ratio to get best performance.

(c) Set up the experiment devices. Set filling ration and power input as variables, then apply different working fluids, water, methanol, ethanol and so on.

(d) Data analysis. Although numerous experiment data are available in literatures, considering there geometry size, it is useless to compare my data with others. But comparison between our own experiment data and own simulation results is conducted.

(e) Apply new working fluids experimentally: nanofluids, azeotrope and fluids mixtures.

Chapter 2

Heat Transfer Mechanism in Thermosyphon

Thermosyphon has complex heat transfer mechanism. Geometrically, it contains three parts, condenser, adiabatic section and evaporator, and each of them has three possible mechanism, natural convection, nucleate boiling and transit convection between these two. In evaporator, it has liquid film and liquid pool, more complex than condenser, which only contains liquid film. However, the liquid films in evaporator and condenser have distinct heat transfer mechanism. For these reasons, in this chapter, detailed mechanism will be discussed. Many empirical equations will be reviewed. This chapter is the preparation for next chapter, mathematic modeling.

2.1 Heat transfer mechanism in condenser section

In the condenser section of CTPT, the heat transfer mechanism is show in fig 2.1. The vapor goes up, condenses on the pipe wall. In the top of condenser, the film thickness is zero and, because of gravity and more condensation on the interface of film and vapor, the thickness of liquid film increases along the pipe wall. At low film Reynolds Number, less than 5, heat transfer process in film is regarded as only conduction. With more power input, the evaporation and condensation are more intense. As a result, the vapor velocity and film velocity are both accelerated. At the same time, shear stress on interface, which proportions to relative velocity, increases. Finally, fluctuation occurs in laminar film and it increases heat transfer rates. Some researchers have pointed out at Reynolds Number equals to 325, the liquid film transfers to turbulence flow. Although the thickness of liquid film increases, which forms more thermal resistance, the total heat transfer rates is much higher than laminar flow. It is because the heat transfer enhanced by turbulence is enough to compensate that cut down by film thickness[5].

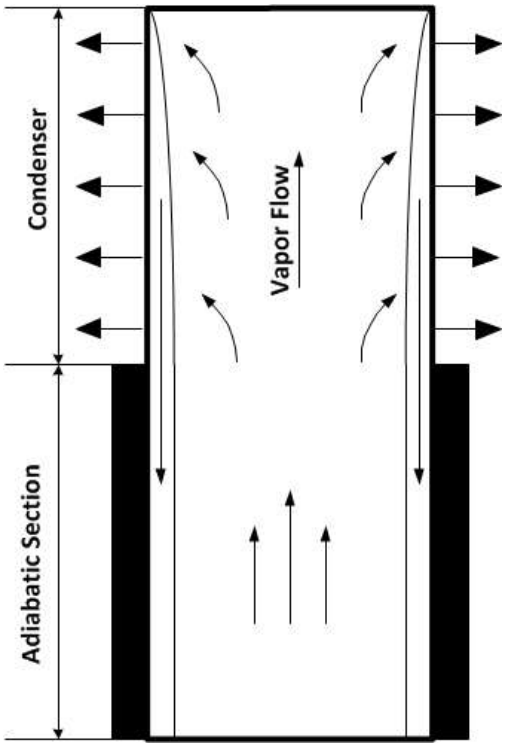

Figure 2.1 A schematic of flow pattern in condenser.

Nusselt's theory about liquid film condensation is widely accepted. In this theory, fluid inertia and the energy convection are neglected. And the average heat transfer coefficient is:

$$h = 0.943[\frac{gh_{fg}\rho_l^2\lambda_l^3}{\mu_l L(T_s - T_w)}]^{1/4} \tag{2-1}$$

Also, we can calculate the average heat transfer coefficient as:

$$h = \frac{\Phi}{\pi dL(T_s - T_w)} \tag{2-2}$$

The Reynolds Number at the exit of condenser is:

$$Re_l = \frac{u_l\delta_{x=L_c}}{v_l} = \frac{\Phi}{\pi d u_l h_{fg}} \tag{2-3}$$

Therefore, from above three equations, we can get formula about Nu and Re_l:

$$Nu^* = \frac{h\delta_{cl}}{\lambda_l} = 0.925Re_l^{-1/3} \tag{2-4}$$

Where, δ_{cl} is the character length of film thickness and it is calculated from the following equation:

$$\delta_{cl} = (\frac{v_l^2}{g})^{1/3}(\frac{\rho_l - \rho_v}{\rho_l})^{1/3} \quad (2\text{-}5)$$

Nusselt's condensation film theory fits the experiment data very well at laminar flow. But when fluctuation happens or in turbulence flow, the analytic value is lower than the experiment data. Some researchers points out multiplying coefficient to strengthen the effect of fluctuation. (Constant value, like$f_{wave} = 1.28$, McAdams; or correlation equation: $f_{wave} = 0.8Re_l^{0.11}$, Zazuli; $f_{wave} = 0.956Re_l^{0.083}$, Uehara; $f_{wave} = 0.842Re_l^{0.33}$, Andros.) [5]

The shear stress comes from two parts, one is friction between vapor and liquid film and another is momentum transfer when vapor condenses. There are bunches of correlation for Nu at turbulence film condensation. According to experiment data, U.S. Engineering Science Data Unit (ESDU) gives out the following correlation for turbulence condensation film:

$$Nu^* = 0.0134Re_l^{0.4} \quad (2\text{-}6)$$

Uehara's group gives out correlations for laminar and turbulence flow respectively:[6]

$$Nu^* = 0.884Re_l^{-1/4} \quad (2\text{-}7)$$

$$Nu^* = 0.044Pr_l^{2/5}Re_l^{1/6} \quad (2\text{-}8)$$

Based on both Uehara's turbulence correlation and Nusselt film theory as well as experiment data analysis, Gross gives out following correlation, which can be applied for both situations:[7]

$$Nu^* = [(f_p Nu^*_{eq.(2-4)})^2 + (Nu^*_{eq.(2-8)})^2]^{1/2} \quad (2\text{-}9)$$

Where,

$$f_p = \frac{1}{1 - 0.63(p^*)^{3.3}} \quad (2\text{-}10)$$

For the above two correlations, $p^* = p/p_{critical}$. Based on this, Gross considered the influence of shear stress and gives out:

$$\frac{Nu^*}{Nu^*_{eq.(2-9)}} = [1 + 4(\tau^*)^2]^{-0.25} \quad (2\text{-}11)$$

$$\tau^* = \frac{\tau}{g(\rho_l - \rho_v)\delta_{cl}} \tag{2-12}$$

The shear stress τ in the above equation is calculated based on different flow pattern.

2.2 Heat transfer mechanism in evaporator section

2.2.1 Introduction

Heat transfer process is quite complex in evaporator in two-phase closed thermosyphon (CTPT) not only because it contains liquid film and liquid pool but also each of them has basically three mechanisms. Neglecting some extreme situations, which will be discussed separately in chapter 2.3, the length of TPCT, l_e, equals to the sum of pool depth, l_p, and film length, l_f.

Three heat transfer regimes are listed in fig 2.2, natural convection, combined convection and nucleate boiling. At lower power input, fig 2.2 (a), the liquid film is continuous and surface fluctuation is not intense. Unlike the film in condenser, the film thickness decreases progressively because evaporation occurs on interface. At high power input, this means more heat flux penetrating liquid film and pipe wall. The formation of bubbles occurs and enlarges on the wall. Because of buoyancy, bubble slides on the pipe wall. Finally, bubbles burst on interface and at the same time some micro liquid droplets will be dispersed into vapor, we call it entrainment phenomenon. Both bubbles and entrainment enhance the heat transfer process, and their heat transfer coefficient is significantly higher than large pool nucleate boiling. Between laminar convection and nucleate boiling, it is combined convection. In this regime, bubbles are also formed but less strong than nucleate boiling.

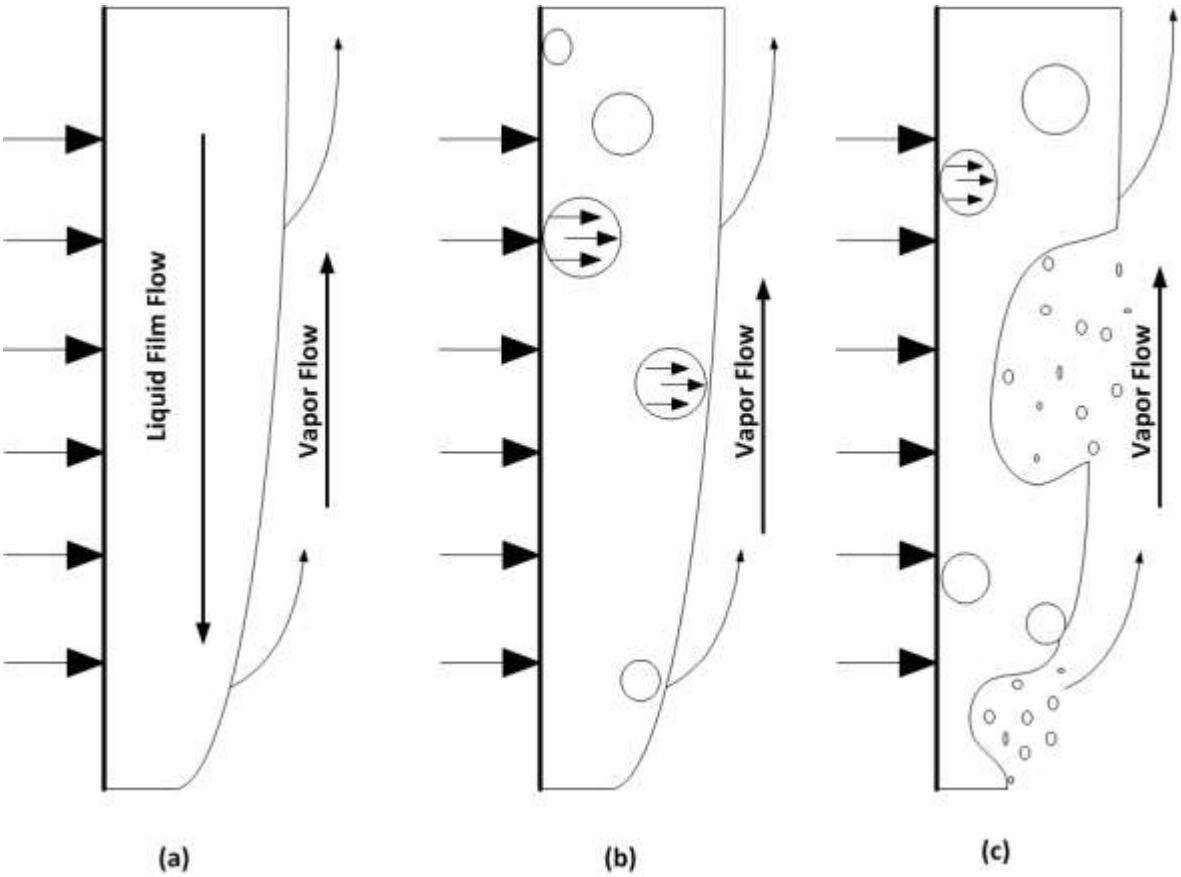

Figure 2.2 A schematic of heat transfer regimes of liquid film in CTPT.

Three pool heat transfer regimes are showed in fig 2.3. Fig 2.3 (a) indicates natural convection in TPCT pool. Heat flux goes through the pipe wall and it makes the near-wall liquid having higher temperature than other parts. While in the middle of liquid pool, the liquid has lower temperature. As a result of density difference, cycling phenomenon happens in liquid pool. Natural convection has low heat transfer coefficient. Some researcher incorporates it into combined convection. Fig 2.3 (c) shows nucleate boiling situation. Lots of bubbles form on pipe wall and pool bottom. They flow up, burst into vapor space and also, the same as liquid film, entrainment phenomenon happens. This makes nucleate boiling has much higher heat transfer coefficient than natural convection. Unfortunately, conventional boiling heat transfer correlation can't be applied directly because they do not account for the mixing effect about bubbles of sliding on the wall and rising from pool bottom. Fig 2.3 (b) shows combined convection, which contains both natural convective cycling and bubble phenomenon.

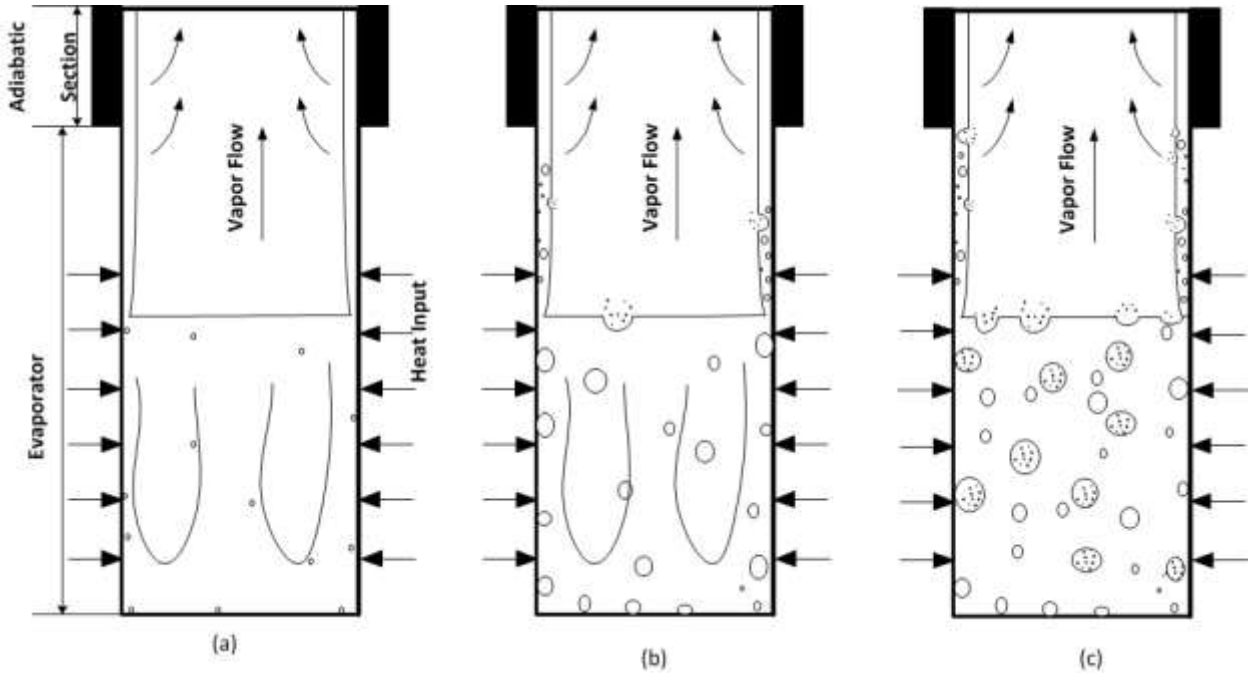

Figure 2.3 A schematic of heat transfer regimes of pool in CTPT.

Because of the complicated heat transfer mechanism discussed above, it is not possible to derive a single correlation incorporating those various processes. Therefore, in the following part lots of correlations will be reviewed and one group of correlations will be the choice in this research.

2.2.1 Review of film correlations

2.2.1.1 Laminar convection

Based on their own data, Shiraishi[8] developed two correlations for laminar and nucleate boiling respectively. It is:

$$Nu_z = 4/3^{1/3} C_1 Re^{-1/3} \tag{2-13}$$

Jialun[9] developed another correlation:

$$Nu_{FL} = 4/3^{1/3} C_2 Re^{-1/3} \tag{2-14}$$

The above two correlations has two different factors. First, $Nu_z$is the local Nusselt number, which means Nu_z's value depends on their location along pipe wall. And Nu_{FL} is the average Nusselt number of the liquid film. Second, $C_1$and C_2 have different calculation method and C_2 is depends on the actual height of liquid pool in evaporator. Both equations are within ±30% of their own experiment data.

2.2.1.2 Nucleate boiling

Shiraishi [8]proposed using the following correlation for liquid film, which is the same equation for liquid pool, when$q_e \geq q_e^*$.

$$h_{NB} = 0.32 \frac{\rho_l^{0.65} k_l^{0.3} {c_{pl}}^{0.7} g^{0.2}}{\rho_g^{0.25} h_{fg}^{0.4} \mu_l^{0.1}} (\frac{P}{P_a})^{0.23} q_e^{0.4} \quad (2\text{-}15)$$

This correlation obtained fairly good agreement with experiment data[10]. For lowerq_e, eqn. 2-15 is applied. q_e^* is the value when the heat transfer coefficient for different regimes are equal, meaning eqn. 2-15 = eqn. 2-13.

$$q_e^* = 2.87 C_1^{1.364} \frac{h_{fg} \rho_l^{0.023} \rho_g^{0.34} k_l^{0.3} g^{0.18}}{l_f^{0.455} \mu_l^{0.318} {c_{pl}}^{0.955}} (\frac{P}{P_a})^{0.31} \quad (2\text{-}16)$$

Jialun proposed his own nucleate boiling film correlation and transition criteria:

$$h_{NB} = 0.0062 C_2^{-1.2} Re^{0.4} Pr_l^{1.25} \lambda_l (\frac{v_l^2}{g})^{-1/3} \quad (2\text{-}17)$$

$$q_e^* = 291.9 C_2^3 \frac{\mu_l h_{fg}}{l_f} Pr^{-1.7} \quad (2\text{-}18)$$

This is for average heat transfer coefficient and it cannot be applied directly as they require a prior knowledge of the liquid pool height.

Other researchers developed many correlations. Unfortunately, seldom correlation is the one widely accepted because of their distinct liquids, geometry sizes and even power input.[11, 12]

2.2.2 Review of pool heat transfer correlations

2.2.2.1 Natural convection

Usually natural convection data are neglected or incorporated in to other heat transfer regime. Thus, there is little empirical correlation directly showing natural convection.

2.2.2.2 Combined convection

Based on thousands of experimental data which covers wide range of working fluids, geometry sizes and power input, GroB proposed [13] his two-phase convection correlation:

$$h_{TC} = 4(\frac{k_l}{d_i})(ArFr^{0.5})^{1/3} Pr_l^{0.5} (\frac{Bo}{10})^n \tag{2-19}$$

Where n=0.5 for Bo≤10 and n=1/6 for Bo > 10. This correlation agrees with GroB's experimental data within ±30%. But for some data, it deviates from the data by ±50%.When applying its dependence of heat transfer coefficient on heat flux, the correlation is:

$$h_{TC} = \frac{4}{10^n} q_e^{\frac{1}{3}} (\frac{k_l^{0.5} Cp_l^{0.5} \rho_l^{\frac{1}{6}} d_i^{\left(n-\frac{1}{6}\right)}}{\mu_l^{\frac{1}{6}} \sigma^{0.5n} h_{fg}^{\frac{1}{3}}}) ((\rho_l - \rho_g) g)^{0.5n+1/6} \tag{2-20}$$

2.2.2.3 Nucleate boiling

Imura [10] proposed their correlation about pool nucleate boiling by multiplying a pressure correction factor, $[1.2(p/p_a)^{0.3}]$, to a correlation for open thermosyphon:

$$h_{NB} = 0.32 \frac{\rho_l^{0.65} k_l^{0.3} Cp_l^{0.7} g^{0.2}}{\rho_g^{0.25} h_{fg}^{0.4} \mu_l^{0.1}} (\frac{p}{p_a})^{0.3} q_e^{0.4} \tag{2-21}$$

As mentioned above, Shiraishi [8] developed their correction for average heat transfer coefficient pool:

$$h_{NB} = 0.32 \frac{\rho_l^{0.65} k_l^{0.3} Cp_l^{0.7} g^{0.2}}{\rho_g^{0.25} h_{fg}^{0.4} \mu_l^{0.1}} (\frac{P}{P_a})^{0.23} q_e^{0.4} \tag{2-22}$$

Eqn.2-21 and eqn.2-22 looks nearly the same, except the exponent of pressure factor. It is because Shiraishi uses eqn.2-21 to correlate heat transfer data for water, ethanol and R-113. But this equation is lower than the ethanol data of Shiraishi by more than 30%, 12% higher than the R-113 data and more than 30% higher than the water data at lower heat transfer coefficient but within ±10% of the data at higher heat transfer coefficient.[14]

By correcting other researcher's correlation, which originally for general purpose nucleate boiling, GroB [13] proposed his correlation:

$$h_{NB} = 55 q_e^{0.7} (\frac{p_r^{0.12}}{(-log_{10} p_r)^{0.55} \sqrt{M}}) \tag{2-23}$$

Where $p_r$is reduced pressure, $p_r = p/p_c$; $p_c$is critical pressure.

By modifying Roshenow's correlation [15] to fit his own experimental data for water, methanol and R-113, Ueda [16] gave out his correlation:

$$h_{NB} = C_{sf}^{-1.7} Pr^{-1.7} (\frac{Cp_l q_e}{h_{fg}}) (\frac{q_e I_m}{\mu_l h_{fg}})^{-1/3} \quad (2\text{-}24)$$

Based on their own experimental data covering water, R-113 and ethanol with various heat fluxes and filling ratio, Kaminaga [17] gave out nucleate boiling correlation in terms of Kutatelatze's conventional pool boiling:

$$h_{NB} = 22(\rho_g/\rho_l)^{0.4} R^{0.2(1-P_r)} h_{ku} \quad (2\text{-}25)$$

The nucleate boiling correlation of Kutatelatze is:

$$h_{NB} = 6.95 \times 10^{-4} (k_l/I_m) Pr_l^{0.35} (\frac{q_e I_m}{\rho_g h_{fg} \nu_l})^{0.7} (\frac{PI_m}{\sigma})^{0.7} \quad (2\text{-}26)$$

Correlation agreed with Kaminaga's own experiment data very well, ethanol within ±20%, water within ±20% and R-113 within ±30%.

2.2.3 Correlation in the thesis

2.2.3.1 Correlation for liquid film

In this thesis, El-Genk's correlations [18] are applied. These correlations are conducted from totally 305 heat transfer data points from different researchers.

For laminar convection:

$$Nu_z = \left(\frac{4}{3}\right)^{\frac{1}{3}} (Re_z)^{-1/3} \quad (2\text{-}27)$$

For nucleate boiling:

$$Nu_{Ku} = 1.155 \times 10^{-3} N_{\mu f}^{0.33} Pr_l^{0.35} K_p^{0.7} (\frac{q_e I_m}{\rho_g h_{fg} \nu_l})^{0.7} \quad (2\text{-}28)$$

For combined convection:

$$Nu_{CC} = (Nu_z^3 + Nu_{NB}^3)^{1/3} \quad (2\text{-}29)$$

Based on the value of dimensionless film parameter, η, liquid film heat transfer is divided into three regimes.

$$\eta = (\frac{q_e I_m}{\rho_g h_{fg} \nu_l})^2 K_P^2 Re_z / Pr_l \quad (2\text{-}30)$$

For laminar, $\eta<10^9$; for nucleate boiling, $\eta>2.7 \times 10^{10}$ and between these two are combined convection. All these three correlations agree with the experiment data within ±15%.

2.2.3.2 Correlation for liquid pool

For liquid pool, El-Genk's correlations[14] are applied as well. They contain a total of 731 heat transfer data points for constant heat flux cylindrical liquids pool and cover a wide range of pool diameter (6-37mm), pool heights (50-800mm), fluid filling ratios (0.1-0.325) as well as various heat fluxes. All data points are sorted into three heat transfer regimes:

(a) Natural convection:

$$Nu_{NC} = 0.475 Ra^{0.35} (\frac{I_m}{d_i})^{0.58} \quad (2\text{-}31)$$

(b) Nucleate boiling:

$$h_{NB} = (1 + 4.95\Psi) h_{ku} \quad (2\text{-}32)$$

Where,

$$\Psi = \left(\frac{\rho_g}{\rho_l}\right)^{0.4} (\frac{P\nu_l}{\sigma} (\frac{\rho_l^2}{\sigma g(\rho_l - \rho_g)})^{0.25})^{0.25} \quad (2\text{-}33)$$

(c) Combined convection:

$$Nu_{CC} = (Nu_{NC}^4 + Nu_{NB}^4)^{0.25} \quad (2\text{-}34)$$

The above equations are determined based on the dimensionless parameter, X, which is:

$$X = \Psi Ra^{0.35} Pr_l^{0.35} K_P^{0.7} Re_g^{0.7} \quad (2\text{-}35)$$

For $X<10^6$, it is natural convection; for $X>2.1\times10^7$, it is nucleate boiling. Between these two, it is combined convection.

For natural convection and nucleate boiling, the correlations have a good agreement within ±15%. The combined convection correlation is also within ±15% of most data and presents smooth transition between natural and nucleate boiling.

2.3 Heat transfer limit for thermosyphon

There are four operation limits of the performance of TPCTs, Counter Current Flooding Limit (CCFL), Liquid Film Dryout Limit (LFDL), Evaporator Flooding Limit (EFL) and Liquid Starvation Limit (LSL). They are caused by different mechanism but all reduce the heat transfer performance.

2.3.1 Counter Current Flooding Limit

When the heat flux goes beyond the critical value, the entrainment becomes strong enough to restrict the liquid film back into liquid pool, showing in fig 2.4. Then the continuous liquid film would be separated into several rivulets. In the constant heat flux pipe wall case, which is the one in this thesis, heat cannot be transferred to liquid. Then the temperature of these areas will increase dramatically. This is the situation need to avoid.

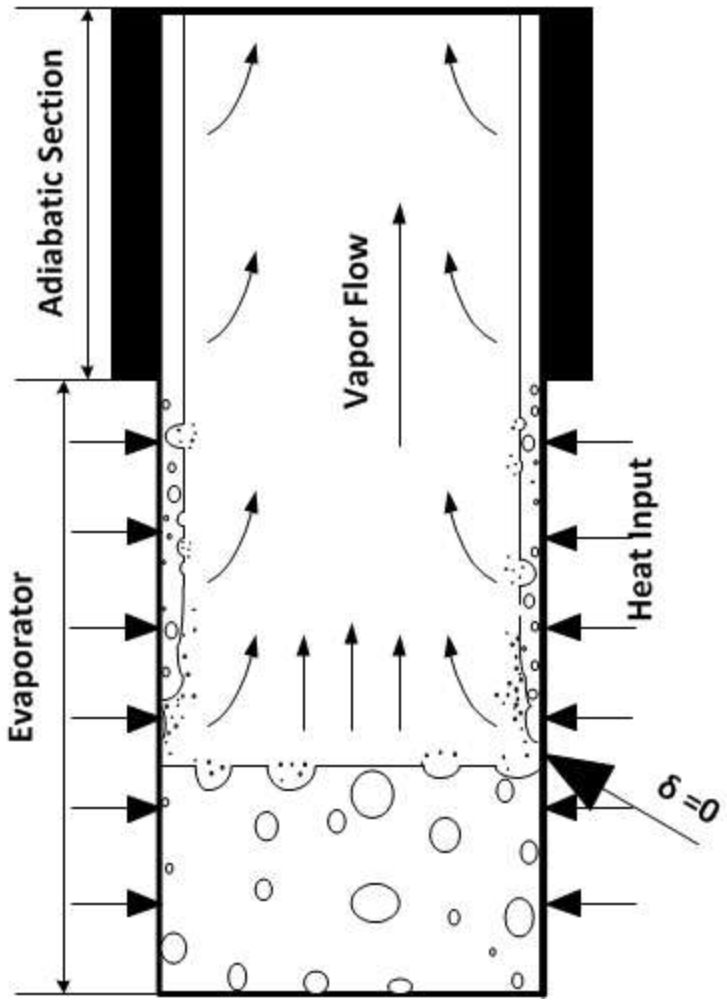

Figure 2.4 A schematic of Counter Current Flooding Limit

El-Genk develops a model to predict the CCFL in thermosyphon and the predictions are in the agreement within ±10%. [19]

2.3.2 Liquid Film Dryout Limit

When the heat flux is extremely large, the evaporation occurs intensely and the thickness of liquid film decrease. After reaching the critical point, the thickness of liquid film above the pool will reduce to zero, showing in fig 2.5. As described above, dryout happens.

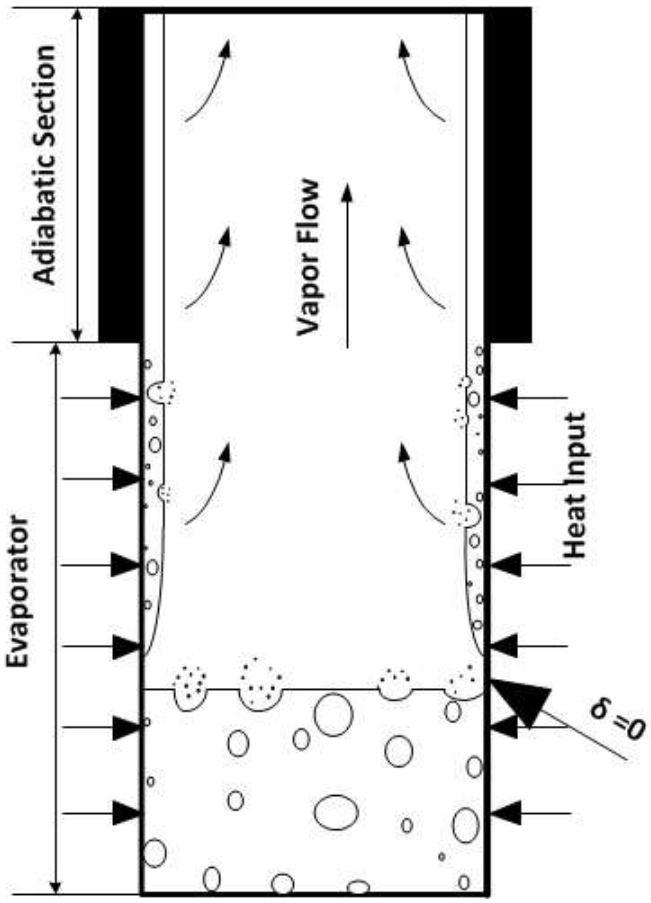

Figure 2.5 A schematic of Liquid Film Dryout Limit

2.3.3 Liquid Starvation Limit

The heat transfer coefficient of liquid film is much larger than that of liquid pool. That means when design the thermosyphon filling ratio should be as low as possible. In this way, thermosyphon has longer film length, l_f. However, we need to consider the Liquid Starvation Limit (LSL), fig 2.6. When running the thermosyphon, the liquid in the pool will evaporate into the upper space and then condense as liquid on the wall flowing back. If the initial filling is too small, the total mass is not enough to supply the liquid film covering the pipe wall. Lacking evaporation cooling, those areas will have extremely high temperature, harmful to whole devices. This is called LSL.

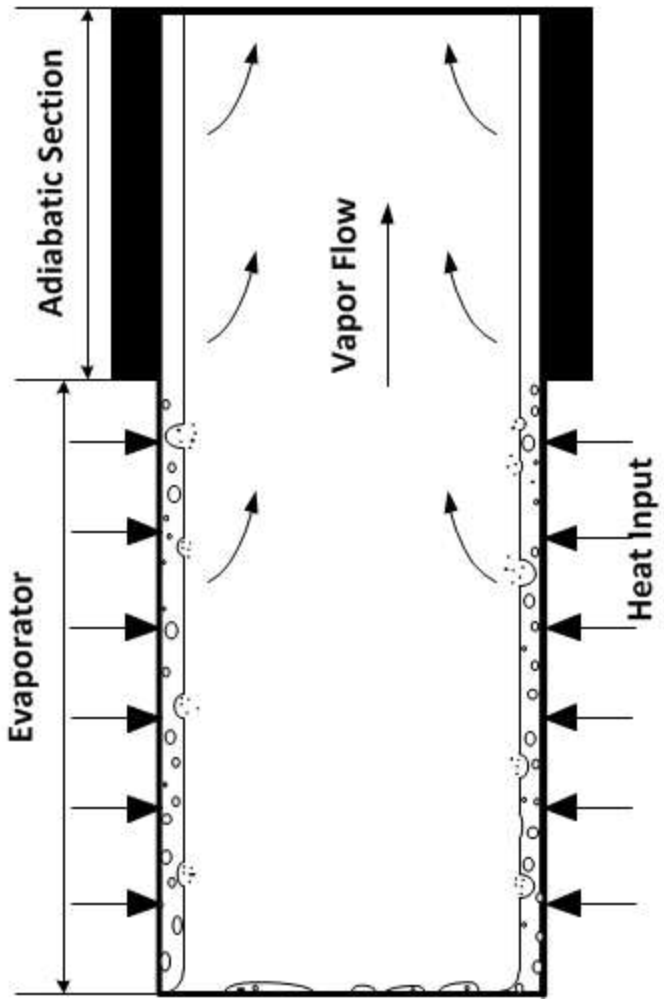

Figure 2.6 A schematic of Liquid Starvation Limit

2.3.4 Evaporator Flooding Limit

Unlike LSL, evaporator flooding limit (EFL) means too much liquid is filled. The liquid will expand when thermosyphon operates. In some extreme cases, the liquid pool level exceeds the evaporator and reaches to adiabatic section. This is no harm to thermosyphon itself but will reduce the thermosyphon performance a lot, in fig 2.7.

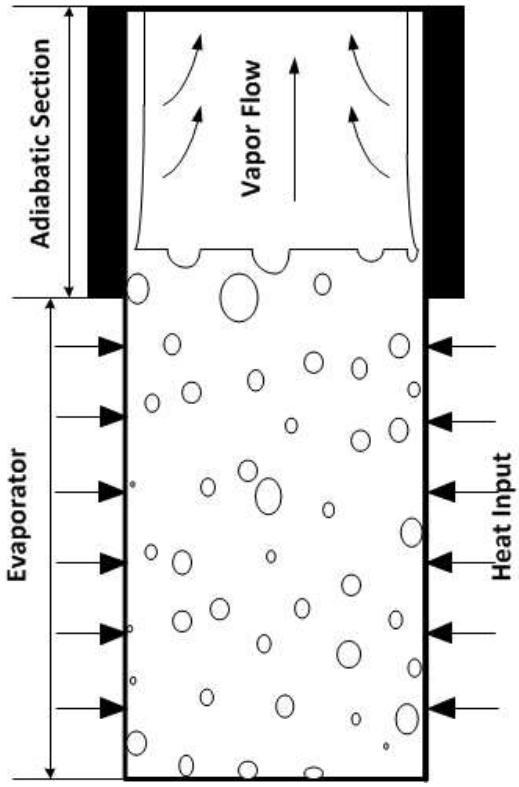

Figure 2.7 A schematic of Evaporator Flooding Limit

Chapter 3

Modeling of Thermosyphon

3.1 Introduction

There are several thermosyphon models developed by different researchers. J. G. Reed and C. L. Tien developed a comprehensive model to predict both the steady-state and transient performance of closed two-phase thermosyphon (TPCT) [20]. El-Genk proposed a thermosyphon model, which is in excellent agreement with ammonia TPCT experiment data. In his model, counter-current flooding limit (CCFL) and dryout can be predicted. B. Jiao also developed a mathematic model and compared with their own experiment data with nitrogen. [21]

In this paper, I review several models, the above three and others, and finally get the mathematic model in my research. First three sections will show the equations in condenser and evaporator separately. Then the detail programming process will be indicated.

3.2 Mathematic model for condenser

Jiao developed her model for liquid film in condenser as follows. In her model, she has five assumptions: (1) fluid inertia in momentum equation and convection term in energy equation are neglected; (2) vapor is incompressible; (3)temperature inside the film is linearly distributed; (4) neglecting the curvature effect of film; (5) average vapor velocity is equal to that at film-vapor interface.

$$\left(\frac{3C_1}{32}+\frac{C_2}{4}\right)C_3\delta^4-\frac{\tau_i}{\mu_l}\left(\frac{C_1}{9}+\frac{C_2}{3}\right)\delta^3=x \tag{3-1}$$

Where,

$$C_1=\frac{\rho_l c_p}{\lambda_l},\qquad C_2=\frac{\rho_l h_{fg}}{\lambda_l(T_s-T_w)},\qquad C_3=\frac{\rho_l g}{\mu_l}$$

And

$$\tau_i=\tau_f+\tau_m \tag{3-2}$$

τ_i is the shear stress on the film-vapor interface and it has two part: (1) the friction between liquid film and vapor; (2) the momentum exchange when vapor condenses.

$$\tau_i = \frac{C_f}{2}\rho_v(u_i + u_v)^2 \tag{3-3}$$

$$\tau_m = \frac{\lambda_l|T_s - T_w|}{h_{fg}\delta}(u_i + u_v) \tag{3-4}$$

Where u_i is the film velocity on interface and u_v is the vapor velocity:

$$u_i = \frac{(\rho_l - \rho_v)g}{\mu_l}\frac{\delta^2}{2} - \frac{\tau_i}{\mu_l}\delta \tag{3-5}$$

$$u_v = \frac{4q_m}{\rho_v d} \tag{3-6}$$

$$q_m = \frac{\rho_l(\rho_l - \rho_v)g}{3\mu_l}\delta^3 - \frac{\rho_l\tau_i}{2\mu_l}\delta^2 \tag{3-7}$$

C_f is the frictional coefficient and is dependent on vapor-liquid relative velocity Reynolds Number:

$$C_f = \begin{cases} \dfrac{16}{Re_{lv}}, & Re_{lv} < 2000 \\ Re_{lv}^{0.33}/1525, & 2000 \le Re_{lv} < 4000 \\ 0.079Re_{lv}^{-0.25}, & 4000 \le Re_{lv} < 30000 \\ 0.046Re_{lv}^{-0.2}, & 30000 \le Re_{lv} < 10^6 \end{cases} \tag{3-8}$$

Where, $$Re_{lv} = (u_i + u_v)d/\nu_v \tag{3-9}$$

Through the above equations, the film thickness distribution and shear stress can be calculated. Then the mass and heat transfer can be calculated out.

$$M_c = \pi\int_0^{x_c}[(2R\delta - \delta^2)\rho_l + (R - \delta)^2\rho_v]dx \tag{3-10}$$

M_c contains the mass in liquid film and vapor in condenser.

$$Q_c = (T_s - T_{wc})\pi D\sum_{j=1}^{N} h_j dx \tag{3-11}$$

Where, $h_j = \frac{\lambda_l}{\delta_j}$.

Although we know the power input, equal to the power output through condenser, is a constant value, in simulation model, we apply the above equation to set it as a comparable value. Because the T_{wc} is the guessing value, which is updated in every iteration step.

3.3 Mathematic model for film in evaporator

The mathematic model for adiabatic is quiet simple because there is neither condensation nor evaporation happening. And the film thickness can be treated as a constant value, equal to the thickness at the exit of condenser. The mass in adiabatic can be expressed as:

$$M_c = \pi L_a[(d\delta_{c,exit} - \delta_{c,exit}^2)\rho_l + (\frac{d}{2} - \delta_{c,exit})^2\rho_v] \tag{3-12}$$

The film model in evaporator is more complex than that in condenser. There are three distinct model for liquid film, (1) laminar flow; (2) combined convection; (3) turbulence flow. In the numerical calculation, we choose the suitable one according to the dimensionless parameter η, mentioned in 2.2.3.1.

3.3.1 Film model for laminar flow

Using the same method, Jiao [21] developed film model in evaporator at laminar flow condition.

$$x - x_c = \frac{C_4 C_5}{8}(\delta^4 - \delta_a^4) + \left(\frac{C_4 C_6}{3} - \frac{C_5}{6}\frac{\tau_i}{\mu_l}\right)(\delta^3 - \delta_a^3) - \frac{C_6}{2}\frac{\tau_i}{\mu_l}(\delta^2 - \delta_a^2) \tag{3-13}$$

Where,

$$C_4 = \frac{(\rho_l - \rho_v)g}{\mu_l}, \qquad C_5 = \frac{\rho_l c_p}{\lambda_l}, \qquad C_6 = \frac{-h_{fg}\pi D L_e \rho_l}{Q}$$

$$\tau_i = \tau_f - \tau_m \tag{3-14}$$

The equations to calculate τ_f and τ_m are the same as list in chapter 3.2. One thing need to note is that here it is negativeτ_m. Because in evaporator the liquid film is losing mass while in condenser the liquid film is gaining mass from condensation. The shear stress from momentum exchange has different sign.

The mass in this section can calculated by the same equation as eqn.3-1 but different integral range.

$$M_{ef} = \pi \int_{x_a}^{x} \left[(D\delta - \delta^2)\rho_l + \left(\frac{D}{2} - \delta\right)^2 \rho_v \right] dx \tag{3-15}$$

Using the same eqn.3-11, we calculate the heat transfer rate.

3.3.2 Film model for combined convection

The film thickness distribution is expressed as:

$$\delta = \delta_a - \frac{q_e}{\rho_l u_l h_{fg}} (x - x_a) \tag{3-16}$$

u_l is the film velocity at the exit of condenser, which is calculated by eqn.3-6

In chapter 2.3, the evaporator operation limits are discussed. The following equation, showing the film breaks at the flow rate reduces to 1%, is applied to determine the break out point:

$$\mathrm{x} = x_a + \frac{0.99\delta_a \rho_l u_l h_{fg}}{q_e} \tag{3-17}$$

For film in condenser and film at laminar flow situation in evaporator, we use eqn.3-11 to calculate heat transfer rate. The physics meaning of this equation is heat conduction through liquid film. However, in higher heat input, this equation is no longer valid because conduction is not the dominant part for heat transfer in this situation. Hence we apply the empirical equation mentioned in 2.2.3.1 to calculate the heat transfer. Mass is calculated by eqn.2-29.

3.3.3 Film model for turbulence flow

The below equation is applied to film thickness calculation for turbulence flow:

$$\frac{d\delta}{dx} = \frac{1}{\rho_l u_l} \left(-\frac{q_e}{h_{fg}} - C_4 \left(\frac{q_e}{h_{fg}}\right)^{2.5} \left(\frac{\delta}{\sigma \rho_v}\right)^{0.75} \right) \tag{3-18}$$

Liquids have their own C_4 value. For R-113 and R-11, C_4 is 663 and 133 respectively; for water, C_4 is 477. [22] Heat transfer rate is by equation in chapter 2.2.3.1. And mass calculation for turbulence flow is by eqn.3-15.

3.4 Mathematic model for pool in evaporator

Liquid pool heat transfer is very difficult because there is seldom any analytical model for it. First, there are many bubbles in liquid pool and this will affect the pool level and mass calculation. Secondly, liquid

will expand after temperature rising, in return affecting the film length. In this section, many empirical equations are used to complete the model.

The void fraction or volumetric concentration can be expressed as: [23]

$$\alpha(\mathrm{x}) = \frac{J_v(x)}{C_o J_v(x) + V_{vj}} \tag{3-19}$$

Where, C_o is distribution parameter,

$$C_o = 1.2 - 0.2\sqrt{\frac{\rho_v}{\rho_l}} \tag{3-20}$$

The drift velocity V_{vj} is calculated by the following process:

$$V_{vj}^{+} = \frac{V_{vj}}{[\frac{\sigma g(\rho_l - \rho_v)}{\rho_l^2}]^{0.25}} \tag{3-21}$$

At low viscosity,$N_{\mu f} < 2.25 \times 10^{-3}$

$$V_{vj}^{+} = 0.03(\rho_l/\rho_v)^{0.157} N_{\mu f}^{-0.562}, \qquad d_h^{+} \leq 30 \tag{3-22}$$

$$V_{vj}^{+} = 0.0019(d_h^{+})^{0.809}(\rho_l/\rho_v)^{0.157} N_{\mu f}^{-0.562}, \qquad d_h^{+} > 30 \tag{3-23}$$

At high viscosity, $N_{\mu f} \geq 2.25 \times 10^{-3}$

$$V_{vj}^{+} = 0.92(\rho_l/\rho_v)^{0.157} \tag{3-24}$$

Where,

$$d_h^{+} = d_h\sqrt{\frac{g(\rho_l - \rho_v)}{\sigma}} \tag{3-25}$$

$$\mathrm{N}_{\mu f} = \frac{\mu_l}{\sqrt{I_m \sigma \rho_l}} \tag{3-26}$$

$$I_m = \sqrt{\frac{\sigma}{g(\rho_l - \rho_v)}} \tag{3-27}$$

Integrating eqn.3-19, we can get the void fraction value.

At$L_p \leq L_e$,

$$\alpha = \frac{1}{C_o} + \frac{\rho_v dh_{fg}}{4q_e L_e} \frac{V_{vj}}{C_o^2 (L_p/L_e)} \ln\left\{ \frac{V_{vj}}{C_o \left[\frac{4q_e L_e}{\rho_v dh_{fg}}\right]\left(\frac{L_p}{L_e}\right) + V_{vj}} \right\} \tag{3-28}$$

At$L_p \geq L_e$, the above equation is still valid for the section in evaporator. For the section in adiabatic section, the following equation is applied,

$$\alpha_e = \frac{\frac{4q_e L_e}{\rho_v dh_{fg}}}{C_o \frac{4q_e L_e}{\rho_v dh_{fg}} + V_{vj}}, \qquad L_p > L_e \tag{3-29}$$

After getting the void fraction, the mass in liquid pool can be calculated,

$$M_p = \pi(\frac{d}{2})^2 L_p[\alpha\rho_v + (1-\alpha)\rho_l], \qquad L_p \leq L_e \tag{3-30}$$

$$M_p = \pi(\frac{d}{2})^2 \{L_p[\alpha\rho_v + (1-\alpha)\rho_l] + (L_p - L_e)[\alpha_e\rho_v + (1-\alpha_e)\rho_l]\}, \qquad L_p > L_e \tag{3-31}$$

The empirical equations in section 2.2.3.2 are used to calculate the heat transfer rate in liquid pool.

3.5 Calculation Process

3.5.1 Thermosyphon logic diagram

Fig 3-1 shows how model is built. Program is built on MATLAB platform. In the main function, as below, power input Q, filling ratio ξ as well as thermosyphon geometry information are input. Condenser model and evaporator model cannot run parallelly because evaporator model needs the results from condenser model.

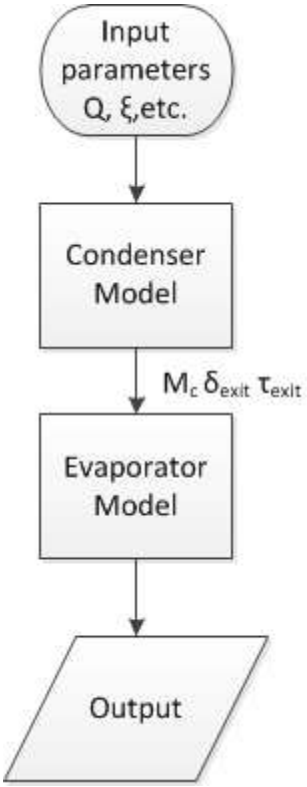

Figure 3.1 Logic diagram for total thermosyphon model

3.5.2 Condenser Model

The calculation process for condenser part is showing in fig 3-2:

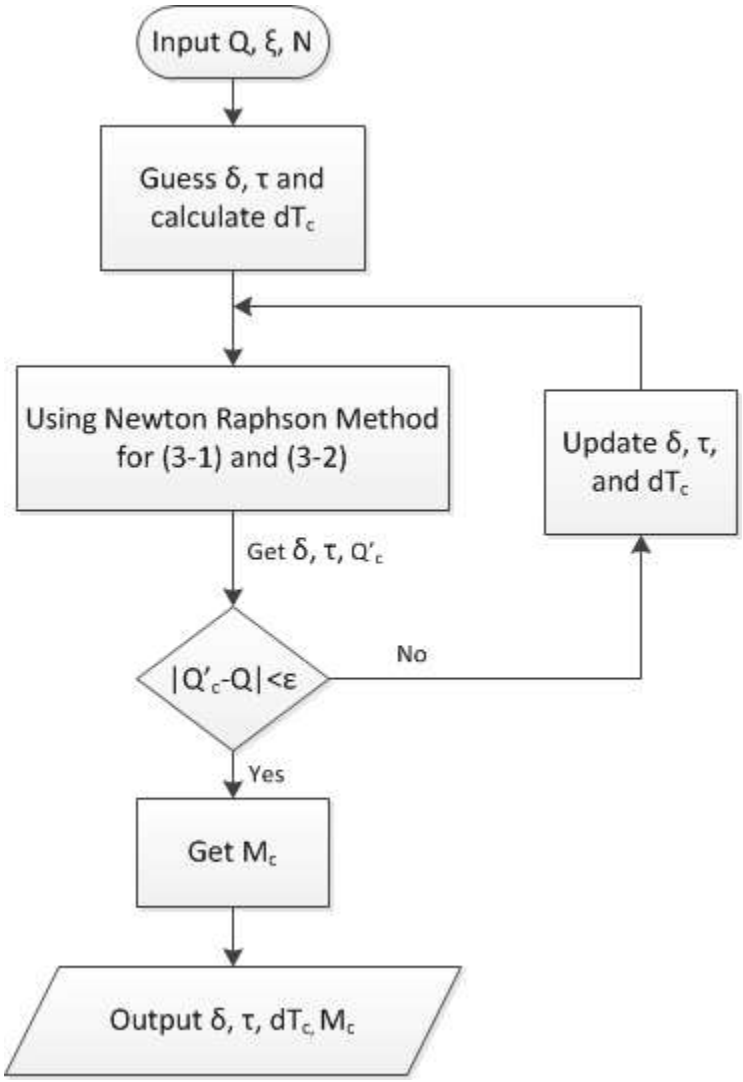

Figure 3.2 Logic diagram for condenser model

(1) Input total power Q, filling ratio ξ, film section number N. Film thickness increases continuously along the pipe wall. To solve this problem, liquid film is divided into N parts, which means in the calculation there will be N data points along the pipe wall and each points can be calculated out separately.

(2) Guess thickness and shear stress for the above N points; calculate temperature different between inner pipe wall and vapor saturate temperature dT_c.

(3) Solve eqn.3-1 and eqn.3-2 with Newton-Raphson method. This will give out new thickness distribution δ and shear stress τ for every point.

(4) Compare the total calculated heat with input power If they are not equal, calculate the new dT_c. Together with δ and τ, repeat step (3). If yes, go to step (5).

(5) Output all results.

3.5.3 Evaporator model

Mass balance and heat balance are cues in this model. Fig 3-3 shows the process for evaporator calculation process:

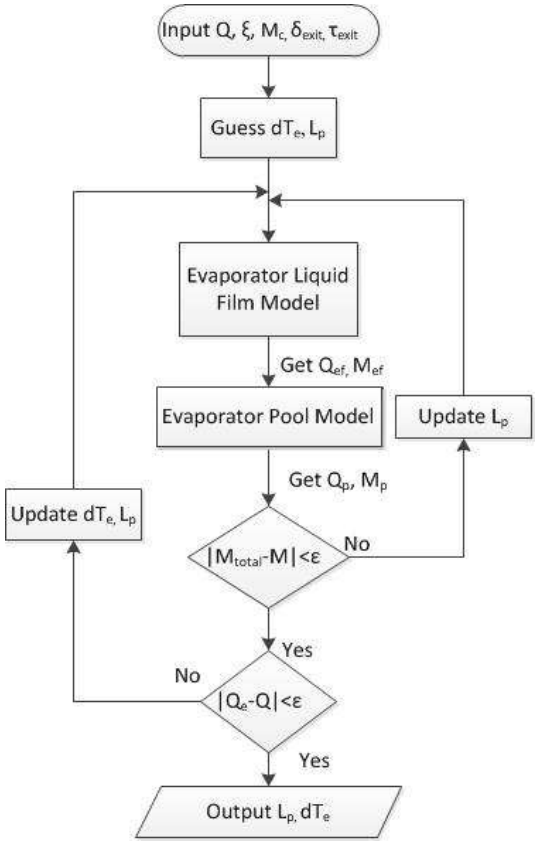

Figure 3.3 Logic diagram for evaporator model

(1) Input parameters. Calculate the total mass M by filling ratio ξ. The thickness and shear stress at exit of condenser, δ_{exit} and τ_{exit}, is also necessity for evaporator model.

(2) Run evaporator film model and get total mass in thermyphon, $M_{total}=M_p+M_{ef}+M_c+M_a$, and total calculating power $Q_e= Q_p+Q_{ef}$.

(3) After mass balance comparison, if not, update the liquid pool length and repeat step (2). If yes, go to step (4).

(4) Heat balance. If the calculated power equal to the power input, go to step (5). If not, repeat step (2).

(5) Output the Results.

3.5.3.1 Evaporator film model

Fig 3-4 gives the calculation process for evaporator film model:

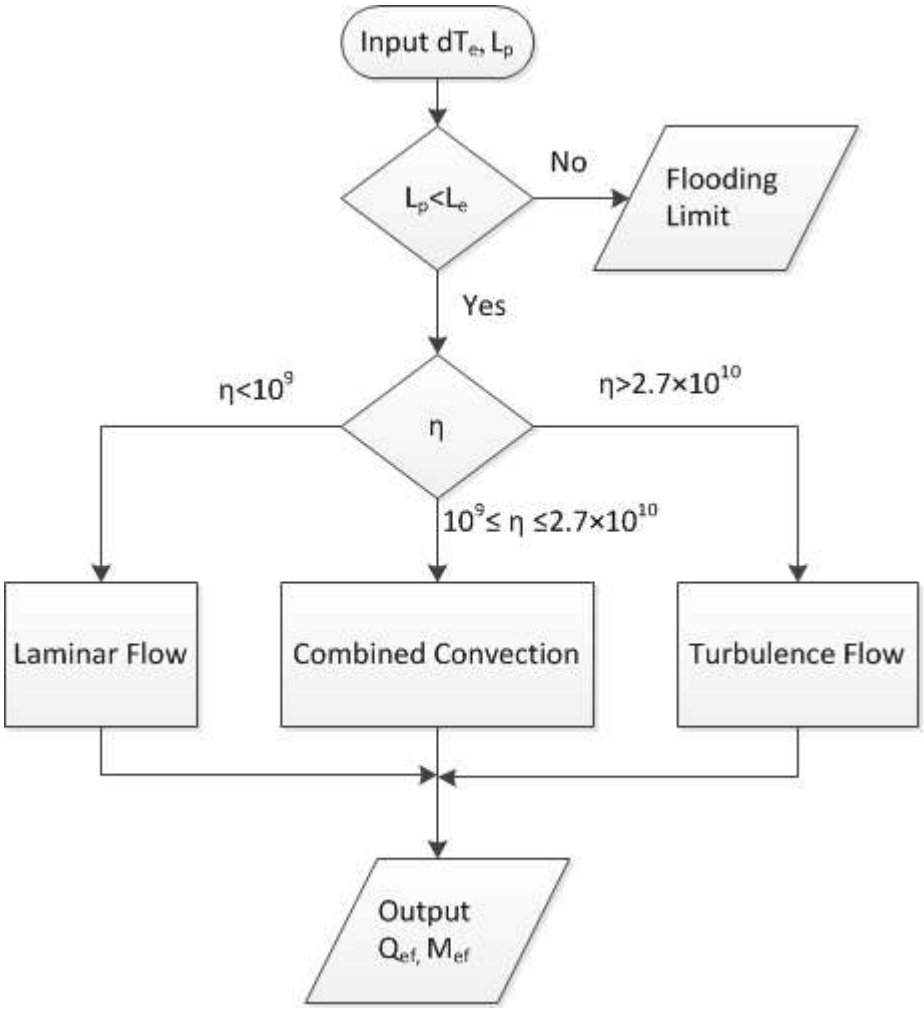

Figure 3.4 Logic diagram for evaporator film model

(1) Input parameters.

(2) Determine whether the operation limit happens.

(3) According to dimensionless parameter, choose different correlations. If it is laminar flow, apply eqn.3-13 and eqn3-14 for thickness, eqn.3-11 for heat transfer rate and eqn.3-15 for mass. If it is combined convection, apply eqn.3-16 for thickness distribution, eqn.2-29 for heat transfer and qen.3-15 for mass. If it is turbulence, apply eqn.3-18 for thickness distribution, eqn.2-28 for heat transfer and eqn.3-15 for mass.

(4) Output M_{ef}, Q_{ef}.

3.5.3.2 Evaporator pool model

Fig 3-5 shows the pool calculation process:

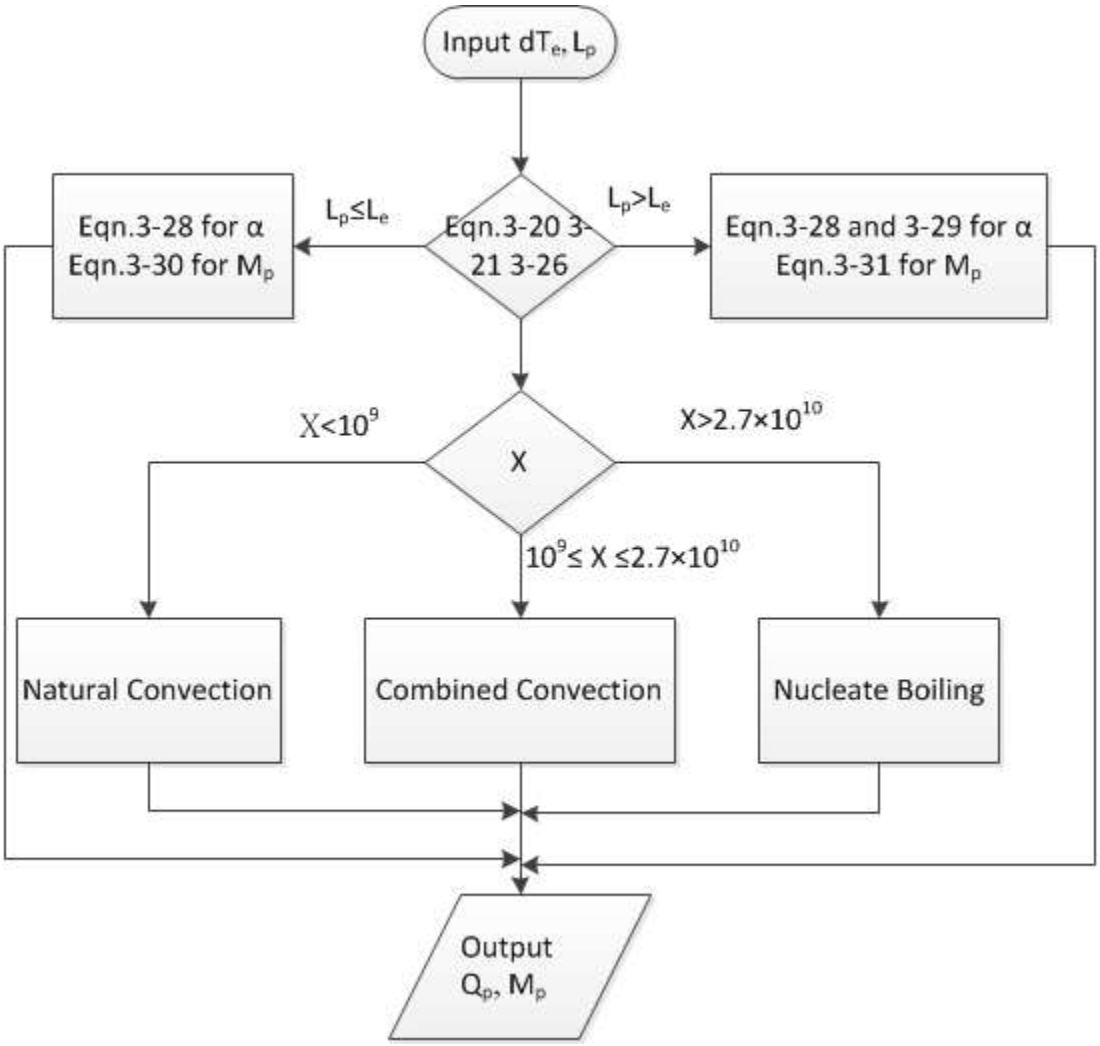

Figure 3.5 Logic diagram for evaporator pool

(1) Input parameters. These parameters are the same as that for evaporator film.

(2) According to the liquid pool length, calculate void fraction α and α_e. Then, apply eqn.3-30 and eqn.3-31 calculating M_p.

(3) According to dimensionless parameter X, calculating heat transfer rate Q_p with eqn.2-31, eqn.2-34 and eqn.2-32 for natural convection, combined convection and nucleate boiling respectively.

(4) Send the results to evaporator model for iteration.

3.6 Results

The program is suitable for all liquids. The following charts and figures indicate results from our thermosyphon model. All thermosyphon operation status can be obtained from this model, including temperature difference both in condenser T_c and evaporator T_e, liquid pool length L_p as well as film thickness distribution.

3.6.1 Methanol Results

The following lists the simulation input,

Fluids	Operation Temp. [℃]	Geometry [m]
Methanol	5	L_c=0.5, L_a=0.2, L_e=0.5, di=0.02

Table 3.1 Simulation results for methanol

Power Input (W)	Filling Ratio	dT_c[℃]	dT_e [℃]	Lp [m]
100	0.1	0.89	1.09	0.044
	0.2	0.89	1.56	0.143
200	0.1	2.26	2.62	0.045
	0.2	2.26	2.73	0.192
300	0.1	3.93	2.24	0.05
	0.2	3.93	3.75	0.229

Fig. 3-6 and Fig. 3-7 show the thickness distribution in condenser and evaporator respectively. Its operation condition is the as above chart but the filling ratio is 0.2 and power input is 100W.

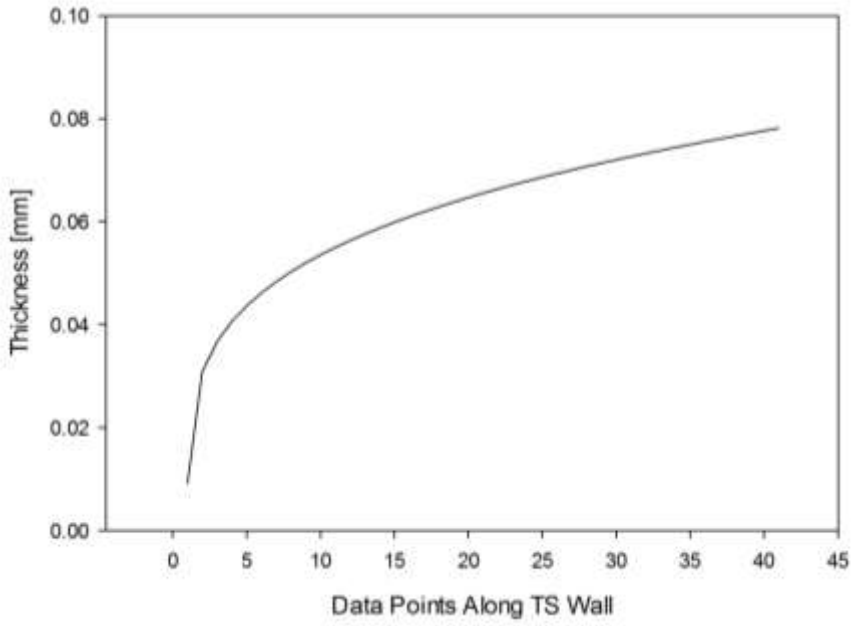

Figure 3.6 Film thickness distribution in condenser

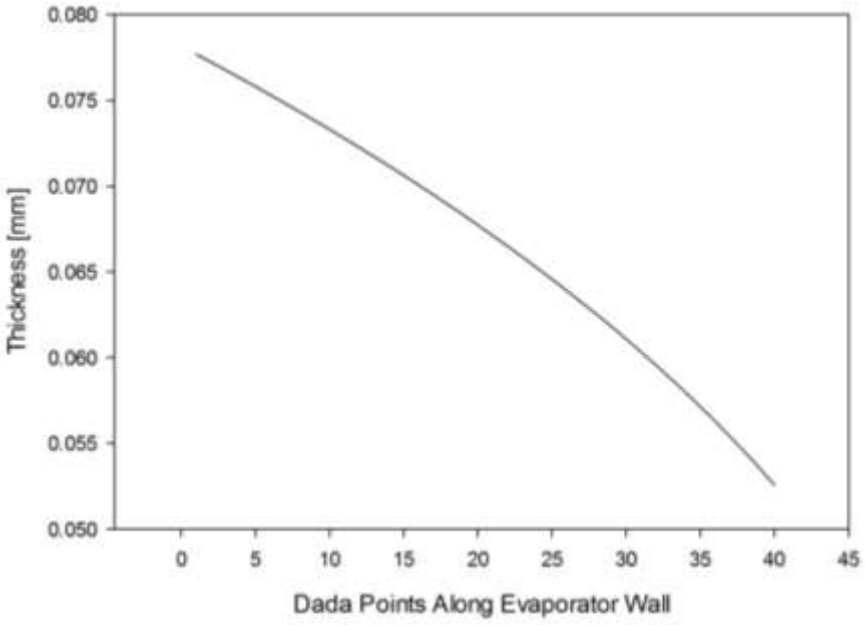

Figure 3.7 Film thickness distribution in evaporator

3.6.2 Ammonia Results

Simulation inputs,

Fluids	Operation Temp. [℃]	Geometry [m]
Ammonia	5	L_c=0.5, L_a=0.2, L_e=0.5, di=0.02

Table 3.2 Simulation results for ammonia

Power Input (W)	Filling Ratio	dTc[℃	dTe [℃	Lp [m]
100	0.1	0.23	0.23	0.04
	0.2	0.23	0.30	0.093
200	0.1	0.58	0.3	0.038
	0.2	0.58	0.4	0.092
300	0.1	1.0	0.34	0.037
	0.2	1.0	0.48	0.093

3.6.3 Water Results

Simulation inputs,

Fluids	Operation Temp. [℃]	Geometry [m]
Water	5	L_c=0.5, L_a=0.2, L_e=0.5, di=0.02

Table 3.3 Simulation results for water

Power Input (W)	Filling Ratio	dT_c [℃]	dT_e [℃]	L_p [m]
100	0.1	0.29	1.18	0.066
	0.2	0.29	3.63	0.25
200	0.1	0.75	2.42	0.079
	0.2	0.75	7.34	0.33
300	0.1	1.33	3.63	0.081
	0.2	1.33	10.5	0.36

3.6.4 Influence of Geometry

To design high efficiency thermosyphon, geometry is important. In this section, condenser length, adiabatic length, evaporator length and tube diameter are discussed as univariate parameter. Basically, the working fluid is methanol running at 5 ℃. The power input is 100 W and the initial filling ratio is 0.1. As the standard group, the geometry is listed in the following chart,

Fluids	Power Input [W]	Operation Temp. [℃]	Filling Ratio	Geometry [m]
Methanol	100	5	0.2	L_c=0.5, L_a=0.2, L_e=0.5, di=0.02

3.6.4.1 Influence of condenser length

The condenser length, L_c, ranges from 0.3m to 0.7. From the following chart, it shows that larger condenser length can reduce the temperature difference both in condenser and evaporator. For longer condenser, it means the surface of heat sink has increased. Thus the dT_c decrease a lot with L_c increasing. At the same time, more liquid and vapor working material stay in condenser part. As the total mass is constant, the liquid pool level would decrease. As mentioned above, liquid film has much larger heat transfer coefficient than pool. Finally, it increases the liquid film length in evaporator even the evaporator length doesn't change and the performance has been improved.

Table 3.4 Influence of condenser length on TS performance

L_c [m]	dT_c [℃]	dT_e [℃]	L_p [m]
0.30	1.49	1.13	0.048
0.40	1.11	1.11	0.046
0.50	0.89	1.10	0.044
0.60	0.74	1.09	0.042
0.70	0.63	1.08	0.040

3.6.4.2 Influence of adiabatic section length

The following data show that the adiabatic section length has no effect on dT_c and has little positive effect on dT_e because larger adiabatic length will increase evaporator liquid film length.

Table 3.5 Influence of adiabatic length on TS performance

L_a [m]	dT_c [℃]	dT_e [℃]	L_p [m]
0.10	0.89	1.11	0.046
0.20	0.89	1.10	0.044
0.30	0.89	1.09	0.041

3.6.4.3 Influence of evaporator length

Operation ratio indicates the ratio L_p/L_e when thermosyphon is running. Originally, it is 0.1. Because all evaporator length conditions has the same L_a and L_c, the amount of liquid mass in those area are the same. Thus, the smaller L_e conditions have less liquid in pool. In return, they have smaller operation ratio.

On the other hand, larger L_e conditions have more heat transfer area. This is the reason why they have lower dT_e.

Table 3.6 Influence of evaporator length on TS performance

L_e [m]	dT_c [℃]	dT_e [℃]	L_p [m]	Operation Ratio
0.30	0.89	1.70	0.021	0.07
0.40	0.89	1.33	0.032	0.08
0.50	0.89	1.10	0.044	0.09
0.60	0.89	0.94	0.056	0.09
0.70	0.89	0.82	0.067	0.10

3.6.4.4 Influence of diameter

When diameter, D, equals to 0.01, the model gives out error because in the calculation there is not enough liquid to create liquid film along the thermosyphon wall. Larger diameter conditions have lower dT_c and dT_e because the heat transfer areas have been increased.

Table 3.7 Influence of diameter on TS performance

D [m]	dT_c [℃]	dT_e [℃]	L_p [m]
0.010	-	-	-
0.015	1.31	1.54	0.038
0.020	0.89	1.10	0.044
0.025	0.66	0.86	0.046
0.030	0.51	0.70	0.047

Chapter 4

Thermosyphon Experiment

4.1 Introduction

There are many thermosyphon experiment data, covering different work fluids, like nitrogen, water, ethanol, acetone, methanol etc. and ranging from small to large geometry sizes. Jiao[21] conducted the experiment using nitrogen.[21] The filling ratio is set at 4.5%, 6.37%, 10.1%, 11.8%, 13.5%, 15.2%, 18.5% and 20.2%. In that paper, ratio is defined as the filling length to the whole TPCT. The experiment data are in good agreement with their own analytical model. S. Chen[24] conducted their experiment with water and methanol to investigate reflux condensation in TPCT. They got the conclusion that at low Reynolds numbers the data fall below Nusselt prediction while at high Reynolds numbers the condensation heat transfer coefficients are underpredicted. J. He [9] conducted the experiment investigating the boiling liquid pool length in TPCT. Shiraishi [8] conducted the experiment to investigate the heat transfer characteristics of TPCT. The conclusion is (1) the thermal resistance in TPCT is very sensitive to operating pressure, heat flux and initial filling ratio; (2) the pressure difference due to the hydrostatic head in the liquid pool is not negligible at low operating pressure. Ueda [16] also investigated the heat transport characteristics of TPCT with R 113, methanol and water experimentally. They concluded, which is similar to Nusselt's prediction, that the condensation heat transfer coefficient of the cooling section shows a trend to decrease with increasing wall temperature difference. Nondimensional expressions are derived to calculate heat transfer coefficient for both heating and cooling section. These expressions are satisfied with experiment data. Jouhara [25] investigated small diameter TPCT charged with water, FC-84, FC-77 and FC-3283. For some point of view, there is one difficulty that because of different geometry size, the experiment data can't be compared with each other.

In the following section, experiment preparation, operation process and results analysis will be discussed. Simulation results in chapter 3 will be compared with experimental data.

4.2 Experiment

An experimental setup is developed to validate the model results and assess actual thermal performance of thermosyphon. A schematic illustration of the experimental setup is shown in Fig 4-1. It

consists of the thermosyphon, a vacuum pump to evacuate the pipe, a water cooling jacket to remove heat from the condenser, and electrical heating tape around the evaporator. The significant device parameters are listed in Table 4-1.

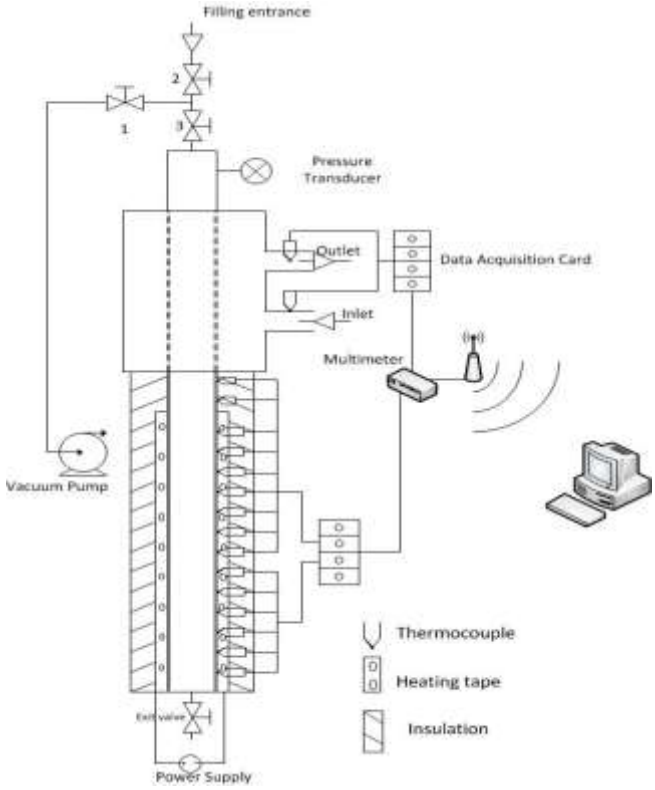

Figure 4.1 the schematic of experiment devices

Table 4.1 Table of device parameter

Parameter	Value
Name:	Methanol
Total Length: L	170 cm
Evaporator Length: L_e	72 cm
Adiabatic Length: L_a	25 cm
Condenser Length: L_c	73 cm
Outer Diameter: D_{in}	2.14 cm

Inner Diameter: D_{out}	2.06 cm

The thermosyphon itself is made from M-type copper tubing and is surrounded by multi-layer insulation. The condenser section is inserted into the water cooling jacket, whose temperature is controlled by a digital chiller. The evaporator section is heated evenly by a heating tape which is controlled by a Variac AC transformer. The axial temperature distribution of the thermosyphon is measured at 15 locations along the thermosyphon using K-type thermocouples. Two of them are located in adiabatic section, and the remaining 13 thermocouples are distributed along the evaporator section. Additionally two high accuracy (±0.05 ℃) RTD probes and a flow meter were inserted in the inlet and outlet of water cooling jacket whose purpose is measure the energy removed from the device in the condenser. A pressure transducer, whose accuracy is ±0.25% FS BSL, is installed above the condenser to monitor the pressure during the whole process. And a thermistor is located around thermosyphon to measure the ambient temperature. The data from all sensors is collected by the Keithley 2701 multimeter and Keithley's ExcelLINX data collection software.

Experiment steps:

1) Vacuum the thermosyphon until the inside pressure goes down to 0 Pa.

2) Close valve 1 and open valve 2 and 3 to fill working fluid. Then leave the whole system for half an hour so that liquid falls down to bottom. Close valve 3.

3) Start up the heating tape at 10 W power input. Then increase to target power input. In our experiment, it costs around 3 minutes to form the liquid film covering the whole pipe wall. So directly heating up to high power input could damage the device.

In this work heat inputs of 50W, 150W, 200W, 225W, and 300W were performed. In all cases, the filling ratio is 0.20.

4.3 Results

4.3.1 Evaporator heat transfer

The temperature difference between the evaporator and the vapor temperature for both the measurement and simulation are shown in Fig. 4-2 for the heat flux range of 50–300W. The model

overestimates the temperature difference at 50W and 150W heat input, and underestimates temperature difference over 200W heat input. At 300W, difference between experiment and simulation is 1.8 ℃, which is the most significant.

The heat transfer regimes predicted by the model for both the liquid film and pool are shown in Table 4-2. The heat transfer region changes from laminar convection to combined convection at around 200W, and continues to change to nucleate boiling at 300W.

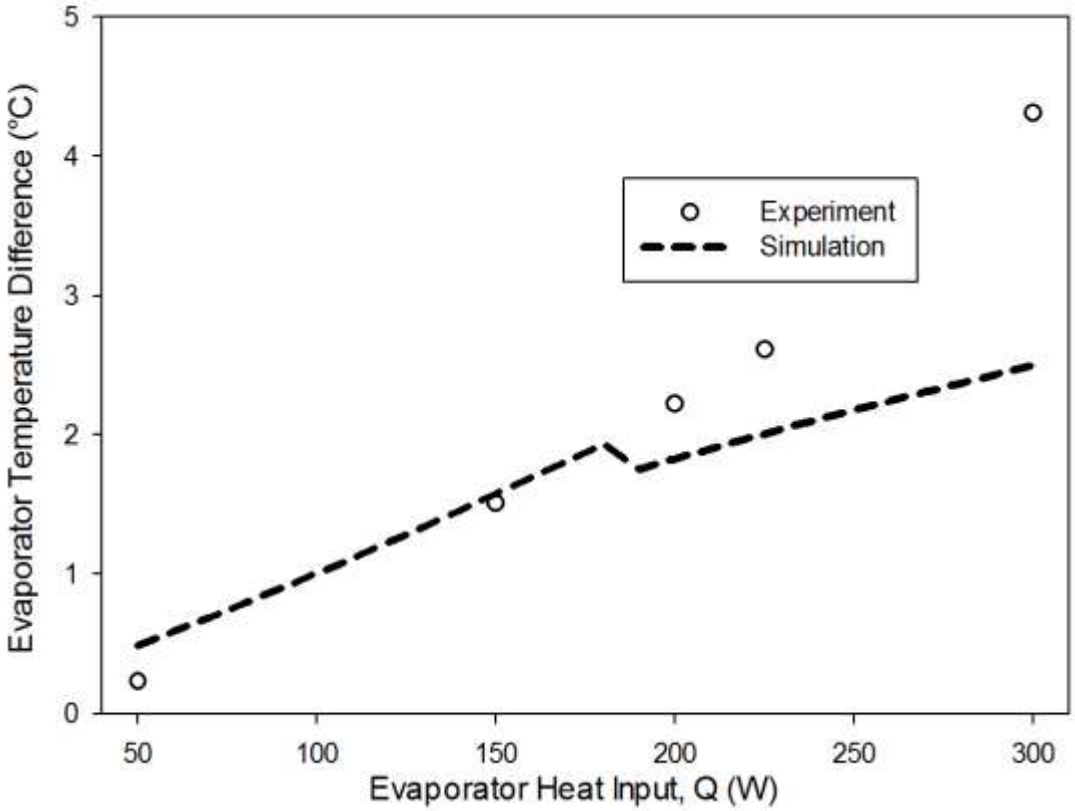

Figure 4.2 Temperature difference of evaporator and vapor

Table 4.2 Heat transfer regime predicted by model

Q	Liquid Film	Pool
50 W	laminar convection	natural convection
150 W	laminar convection	natural convection
200 W	combined convection	natural convection

225 W	combined convection	natural convection
300 W	nucleate boiling	combined convection

4.3.2 Condenser heat transfer

The condenser wall temperature is estimated using the Dittus Boelter correlation[26] for a concentric tube annulus using the water jacket geometry, volume flow rate, and jacket inlet and outlet water temperatures. The difference between the vapor temperature and the condenser wall is then determined. The results for the condenser wall –vapor temperature difference are showing in Fig. 4-3. The simulation results and experiment are in good agreement across the heating power input range. Note also that the temperature drop is smaller than in the evaporator, since there is no liquid pool that can result in large temperature drops.

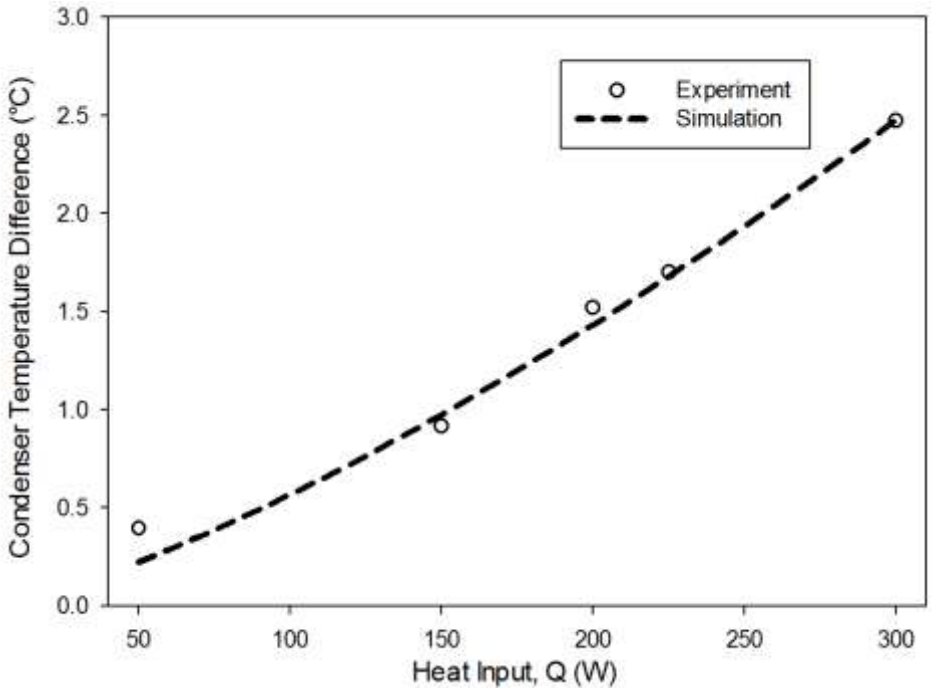

Figure 4.3 Temperature drop in condenser

4.3.3 Overall temperature difference

As discussed earlier, the overall temperature difference, from evaporator to condenser, is a critical value for operation. This value is obtained by combining the evaporator and condenser temperatures. The overall temperature drop versus heat input for both the measurements and simulation are shown in Fig.

4-4. The model overestimates this difference at 50 and 150W heat input, and underestimates it starting from 200W to 300W. This is due to the variation in the evaporator, also seen in Fig. 4-2.

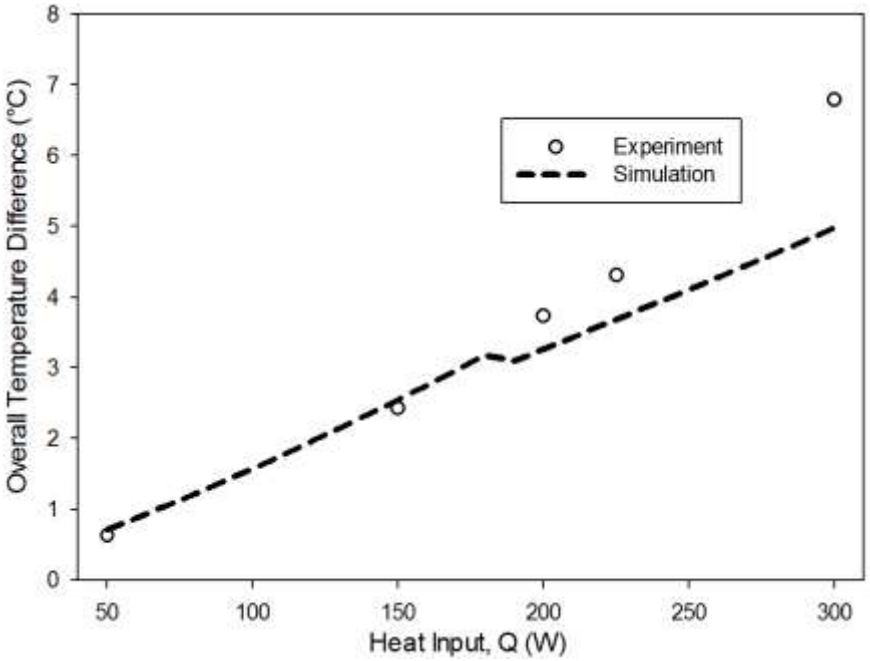

Figure 4.4 Total temperature drop in TPCT

It can be seen that the temperature drop across the thermosyphon device is only several degree Celsius, which is attractive for using these devices in refrigeration applications where minimal temperature drops are required.

4.3.4 Vapor temperature comparison

The experimental results from Ethanol (ranging from10% to 20% filling ratio) and Methanol (from 5% to 25% filling ratio), covering power throughout for 50W, 100W, 200W, 300W, are listed inFig. 1. It shows that at the same power throughout, the vapor temperature is independent of initial filling ratio. In other words, the vapor temperature only changes with power input. This can be explained from the heat transfer process in condenser. When the vapor condenses on the wall, the cooling process is heat conduction through liquid film and pipe wall. It is easy to understand that the liquid film thickness along conderser wall is independent of filling ratio. This is also predicted by our analytical model. So at the same power input, the heat resistance is nearly the same. In our experiment, the cooling jacket is controlled so that the cooling water is at the same temperature for different filling ratio experiment. Therefore, at certain power input, the vapor temperature is the same for different filling ratio.

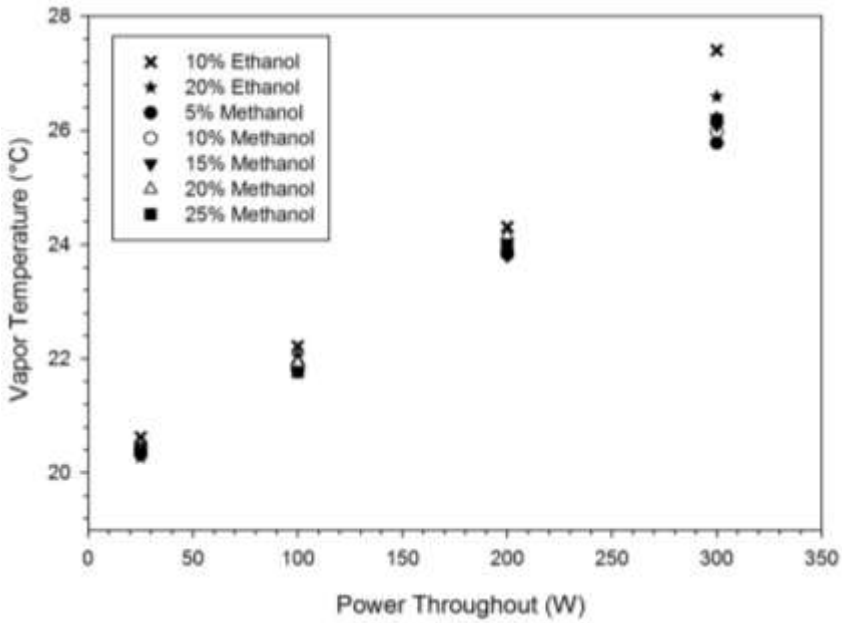

Figure 4.5 Vapor temperature for different filling ratios

4.3.5 Vapor temperature and adiabatic temperature comparison

Fig. 2 shows the temperature comparison between vapor temperature and adiabatic section. Theoretically, these two temperature should be equal, just as the line shows, because in adiabatic section there is no heat transfer and the temperature from the wall is the vapor temperature. However, the material for our device is copper. There is temperature gradient between condenser and evaporator. Heat flux goes up along the pipe wall. The highest error comes from the ethanol data at 300W. The adiabatic section is 0.7 ℃ higher than vapor temperature. This is caused by the heat flux from evaporator. Except this single data, the experiment data indicates that we can treat the adiabatic temperature as vapor temperature and this experiment has relative high accuracy.

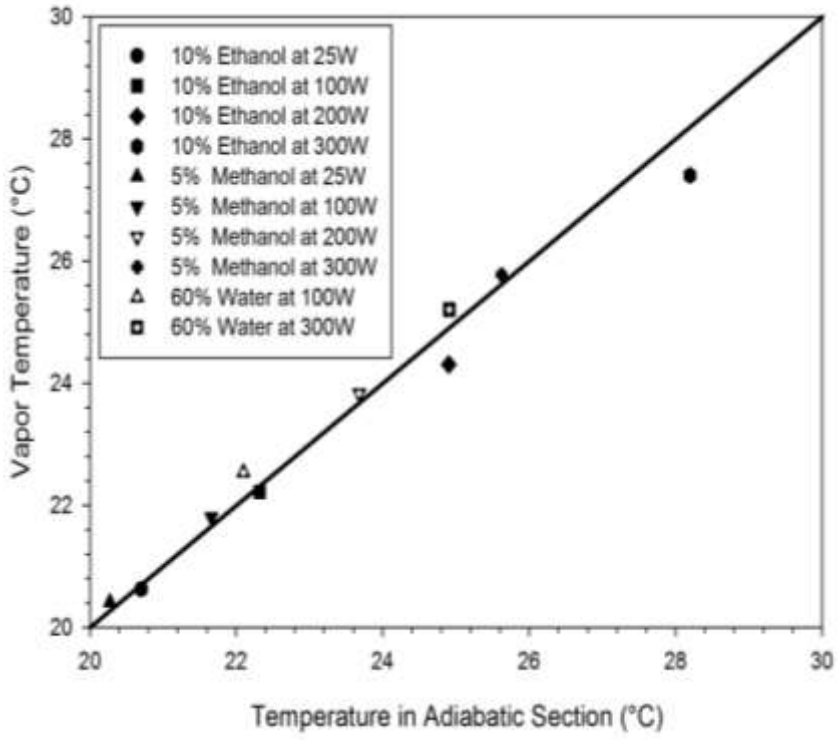

Figure 4.6 Comparison of Adiabatic Temperature and Vapor Temperature

4.3.6 Experiment and simulation results comparison

The evaporator temperature difference equals to temperature difference between outer pipe wall and vapor temperature. Fig. 3 shows its experiment and simulation comparison results for ethanol at 10% filling ratio. It indicates that the experiment and simulation results match very well.

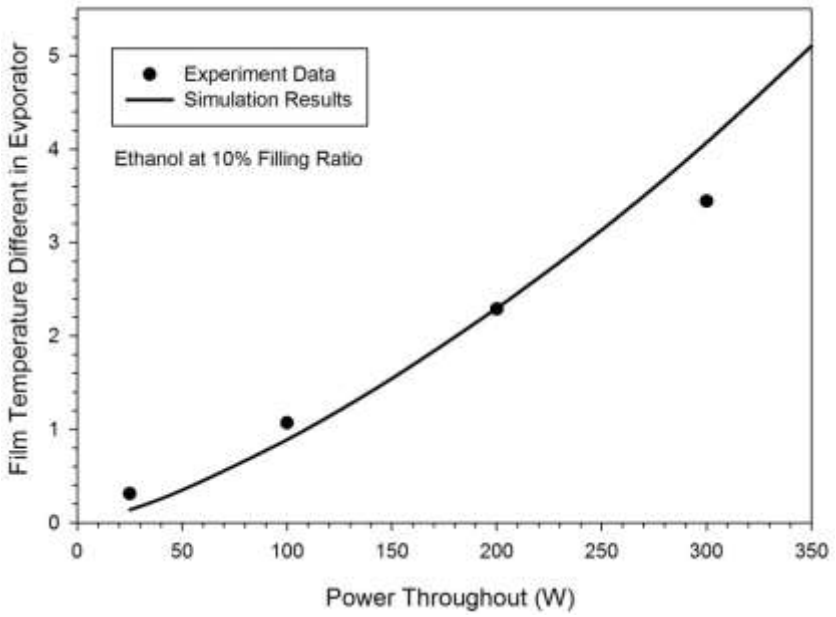

Figure 4.7 Experiment and Simulation Results Comparison of Evaporator Temperature Difference for Ethanol

Fig. 4 shows evaporator temperature different comparison for ethanol at 10% filling ratio. The comparison indicates that experiment and simulation resulats match very well below 200W. Fot High power input, the experiment is larger than simulation results. This may be caused by the simulation curve trendency. In the model, for the whole power input range, the results are not continuous because three heat transfer regimes are divided by parameter η. In fig. 3, curve for ethanol, the simulation results are continuous as there is no heat transfer regime change between 25 and 350W. However, for methanol, for the same power input range, three heat transfer regimes, laminar flow, combined convection, turbulence flow, appears.

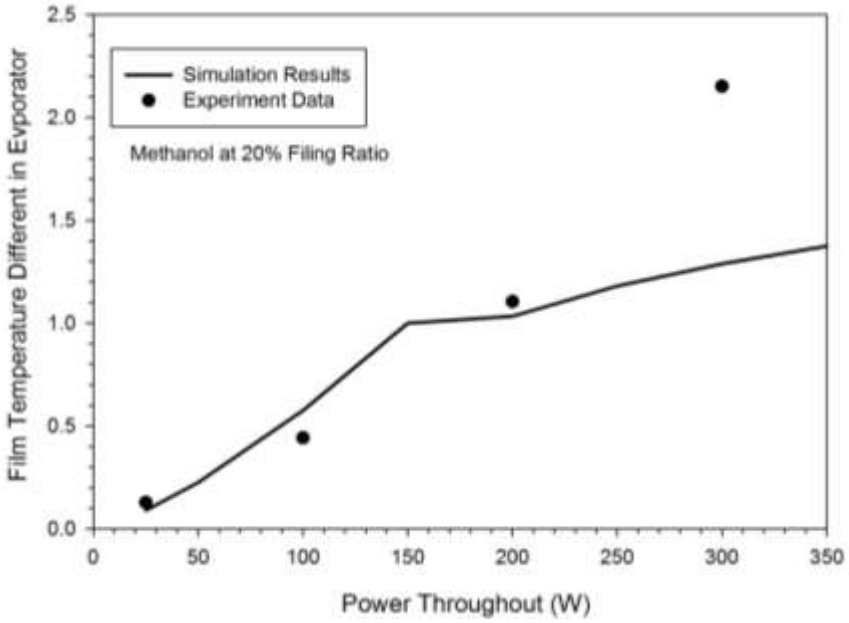

Figure 4.8 Experiment and Simulation Results Comparison of Evaporator Temperature Difference for Methanol

4.3.7 Temperature distribution in evaporator

Fig.5 and Fig. 6 shows the temperature distribution on outer pipe wall of evaporator for methanol and ethanol respectively. In this experiment, totally 13 thermocouples are set, covering along the evaporator from its bottom to top. The x-coordinate shows the distance from local point to thermosyphon bottom. The y-coordinate obviously shows the outer wall temperature. The experiment results demonstrate the analytical model. The first two points have relative high temperature because it is in low heat transfer efficiency area, liquid pool. In the film area, the top has higher temperature and then reduces gradually. This is caused by the film thickness variation as thicker film, the upper area, contributes more thermal resistance.

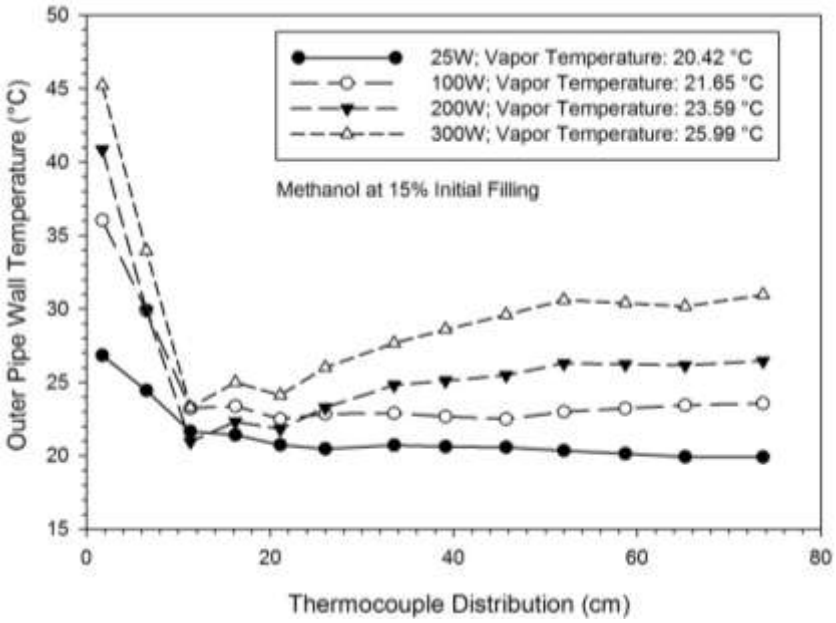

Figure 4.9 Evaporator Outer Wall Temperature Distribution for Methanol

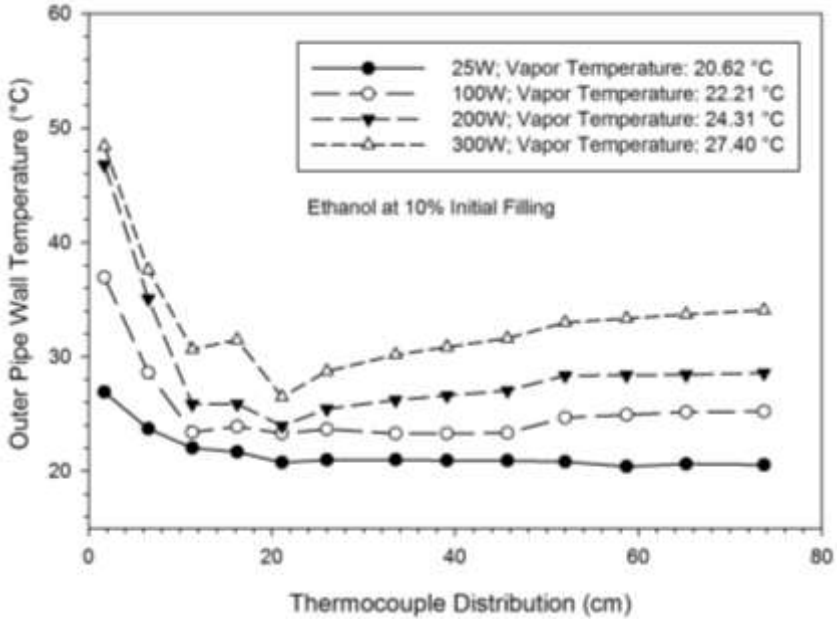

Figure 4.10 Evaporator Outer Wall Temperature Distribution for Ethanol

4.3.8 Operation limits

The operation limits are observed in our experiments, shown in Fig.7 and Fig.8. Two data points are chosen from 13 thermocouples points along TPCT and these two are located in liquid film area. It is expected all 9th temperature should be around 2 ℃ higher than 7th data points. This is true for operation condition above 0.15 initial filling ratios. However, for condition at 0.05 and 0.1 filling ratio, the 7th

temperature is more than 10 ℃ higher than 9th data points. This value is quite constant during operation, neither increasing nor decreasing. In chapter 2.2, heat transfer limits for thermosyphon are discussed. The Counter Current Flooding Limit (CCFL) and Liquid Film Dryout Limit (LFDL) may be the reason to explain the irregular temperature distribution.

In ethanol experiments, this phenomenon is not observed.

Thus, two conclusions are made: (a) at high power throughput condition, low initial filling could cause irregular high temperature distribution in liquid film area; (b) CCFL or LFDL is related to liquid type.

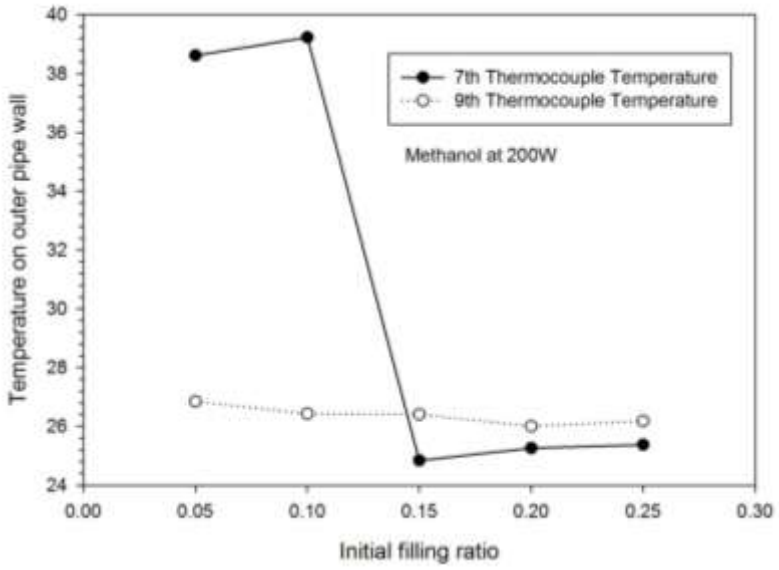

Figure 4.11 Operation limit for methanol at 200W

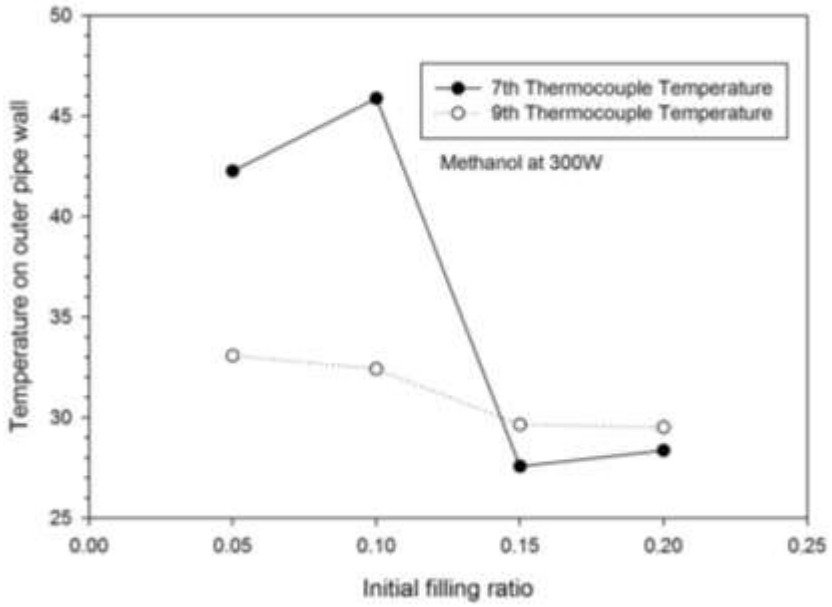

Figure 4.12 Operation limit for methanol at 300W

Figure 9 shows the temperature recordings for 7th and 9th thermocouple for water TPCT at 60% initial filling ratio. 1 to 88 is for 100 W power throughput; 89 to182 is for 200W and the last is for 300W. The time interval for between each recording is 30 seconds.

One phenomenon is that most temperature recording for 9th thermocouple is higher than 7th. This is easy to understand as upper area has thicker film thickness, meaning more thermal resistance. Another finding is that for all power input, the temperature sequence is oscillating, neither constant at low temperature as expectation nor stable at a higher temperature as above operation limits. In detail, for each cycle, to reach the peak, several recording intervals are needed, but down to the valley only needs one interval. Our initial explanation for this phenomenon is that the film is unstable. First, the film covers the wall surface then the thickness reduces gradually and finally breaks. After that, the temperature goes up. Within 30 seconds, the surface is covered by falling liquid film from upper area and temperature goes down.

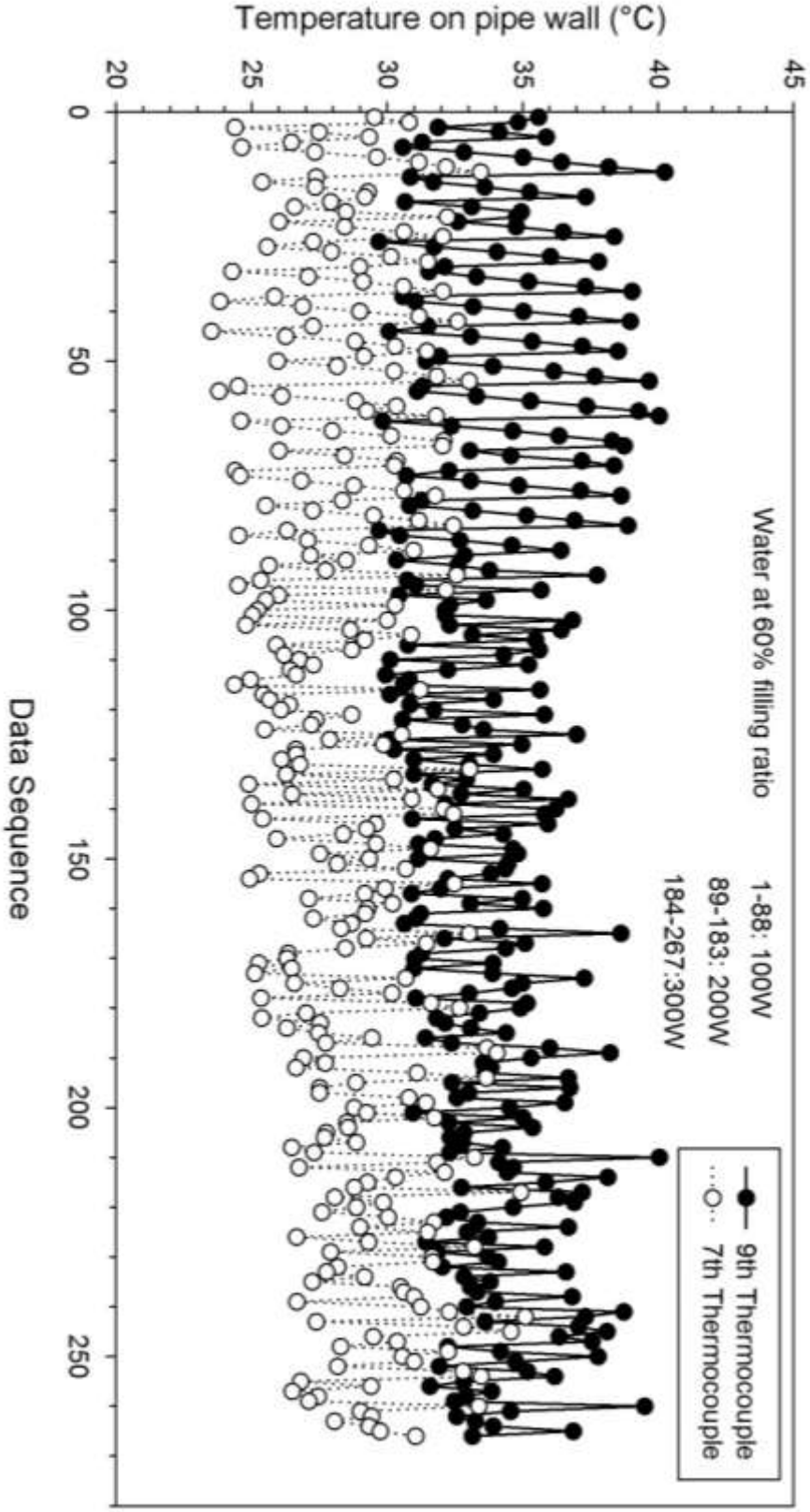
Temperature on pipe wall (°C)
20
25
30
35
40
45
0
50
100
150
200
250
Data Sequence
Water at 60% filling ratio
1-88: 100W
89-183: 200W
184-267:300W
9th Thermocouple
7th Thermocouple

Figure 4.13 Temperature data sequence for water at 60% filling ratio

Chapter 5

Thermosyphon with Nanofluids, Azeotrope and mixture

5.1 Introduction about nanofluids

Conventional working fluids for thermosyphon have been studied for a long time. In this chapter, nanofluids are used as working fluids for thermosyphon experimentally. This is a new method to enhance the TPCT performance.

"Nanofluids" is the name conceived by the researcher in Argonne National Laboratory. It describes a kind of liquid in which nanometer-sized particles (with typical length scales of 1 to 100 nm) are suspended. The base liquids can be water, ethylene glycol, light oils and so on. In most literatures, the Nanoparticle materials in nanofluids are oxide metal (Al_2O_3, CuO, and MgO), nitride ceramics (AlN, SiN), carbide ceramics (SiC, TiC), metals (Ag, Au, Al, Cu, and Fe) and nanotubes (SWCNT, DWCNT).

Many research groups indicate that nanoparticles can enhance the thermal conductivity and convective heat transfer performance of base liquids in experiment field. Also various investigators have proposed physical mechanisms and mathematical models to describe and predict the thermal properties and heat transfer of nanofluids.

In this section, literatures are reviewed, discussing the thermal conductivity and viscosity of nanofluids as well as its mechanism.

5.1.1 Thermal conductivity of nanofluids

Thermal conductivity is one of the most important parameter in heat transfer field. And its value directly influences on heat transfer performance, thus most researchers and literatures are focusing on it. There are seven parametric effects on thermal conductivity of nanofluids: (1) particle volume concentration, (2) particle materials, (3) particle size, (4) particle shape, (5) base fluid material, (6) temperature, (7) additive.

5.1.1.1 Particle volume concentration

Volume concentration is defined as,

$$\varphi = \frac{\frac{W_{particle}}{\rho_{particle}}}{\frac{W_{particle}}{\rho_{particle}} + \frac{W_{base-liquid}}{\rho_{base-liquid}}} \quad (5\text{-}1)$$

Here we use the density of nanoparticle at bulk material instead of its powder density.

Lee[27] and Das[28], both using Al_2O_3 (38mm) with water, show that higher volume concentration could enhance the thermal conductivity more. Lee[27] with CuO (24nm) and Wang[29] with CuO (23nm) shows the same trend. Other literature [30-33] covering nanoparticles size ranging from 12 nm to 60nm and various temperatures also show the trend clear: thermal conductivity enhancement increases with increased particle concentration by 1% to 30%.

At higher particle volume concentrations, the increase in enhancement is expected to diminish or even reverse. However, at the volume range for automotive applications shown in the above literature, this prediction is not found.[34]

5.1.1.2 Particle materials

As mentioned above, various materials can be used in nanofluids. Their effects on thermal conductivity have been discussed. Group number one: Wang (28nm Al_2O_3; 23nm CuO)[29], Lee (24nm CuO)[27], Das (29nm CuO)[28] and Xie (26nm SiC)[30]. The base fluid is water. Their results show that with the volume concentration ranging from 0.4% to 10% these materials have the nearly same thermal conductivity enhancements. Group number two: Xie (15nm Al_2O_3)[30], Eastman (10nm Cu)[35] and Hong (10 Fe)[36, 37]; and the base liquid is ethylene glycol. Their results show that Fe and Cu can reach the same thermal conductivity enhancement, 15%, at much lower volume concentrations.

From the above two experimental results comparison, it is clear that metal nanoparticles can enhance the thermal conductivity of nanofluids more than oxide metal and nitride ceramics. This is because the thermal conductivity of metal is higher than oxide metal and other components.

5.1.1.3 Particle size

Particle size is another important parameter when choosing nanofluids. Three groups of data are compared: (1) Al_2O_3 (38 and 60nm) in water, (2) Al_2O_3 (15 and 38nm) in ethylene glycol and (3) CuO (24 and 29nm) in water.[27, 28, 30] Their results show that larger size particle can enhance thermal conductivity more.

However, if adding another group data from Wang[29], we cannot get the above trend because this paper shows that smaller particle nanofluids can get better results than larger one. Several reasons might explain this: the size information comes from power manufacturer; measurement methods have errors and so on. Neglecting this, the above trend is also contradictory with the current theoretical model, which indicates that smaller particle size has better performance.

5.1.1.4 Temperature

The thermal conductivity is sensitive to temperature. The experimental data of Al_2O_3 in water[28, 33], CuO in water[28, 33] and MWCNT in water[31, 38] support the conclusion that higher temperature could enhance the thermal conductivity increasing. It makes sense because for most liquids, metal and oxide metal they have this trend. However, the experimental data from Masuda [32], Al_2O_3 in water, contradicts this conclusion.

5.1.1.5 Additive

Additives have been used in experiments because they can keep nanoparticles in suspension status and prevent from agglomerating. No specific study focuses on this topic. But most literature results show that additives have positive effect on thermal conductivity

5.1.1.6 Other influences

Some researchers studied the influence of particle shape on thermal conductivity[30, 39]. 26nm sphere, 600nm cylinder and 10×40 nm rod are the compared data. Conclusion is hard to make because in these experiments shape is not the isolated condition.

The base fluid choice has influence on thermal conductivity too. However, this is not the concern in this research, because there are other essential key factors for thermosyphon working fluid choice, like viscosity, vapor density and latent heat. What we do is based on our model in chapter 3 to choose base fluids.

5.1.2 Viscosity of nanofluids

In 1906, Einstein derived the equation to evaluate the effective viscosity of suspension of spheres,

$$\mu_{eff} = (1 + 2.5v_p)\mu_m \tag{5-2}$$

Since then, researchers derive lots of equations to calculate the suspension liquid viscosity. From experimental data, Al_2O_3 in water, CuO in water, MWCNT in water, Al_2O_3 in octane and TiO_2 in water,

they all, obviously, show that viscosity will increase. However, their values are higher than the predicts coming from current simulation model.[34]

5.1.3 Density and specific heat

The density and specific heat of nanofluids can be calculated by simply mixtures: heat balance and mass balance.

$$\rho_{eff} = \frac{m_b + m_p}{V_b + V_p} = \frac{\rho_b V_b + \rho_p V_p}{V_b + V_p} = (1 - \varphi)\rho_b + \varphi \rho_p \tag{5-3}$$

In the same way, get,

$$C_{p\_eff} = \frac{(1 - \varphi)(\rho C_p)_b + \varphi (\rho C_p)_p}{(1 - \varphi)\rho_b + \varphi \rho_p} \tag{5-4}$$

5.1.4 Mechanisms of enhanced thermal conductivity in nanofluids

There is no such a widely accepted mechanism that explains the thermal conductivity enhancement in nanofluids. Simulation results are lower than the experimental data. In Keblinski's work[40], four potential mechanisms were discussed, (1) Brownian motion, (2) liquid layering at liquid/particle interface, (3) nature of heat transport in nanoparticles, (4) effects of nanoparticle clustering.

Brownian motion can be expected to increase thermal conductivity because of solid to solid transportation. However, according to Keblinski's calculation, the thermal diffusion is tens of times faster than Brownian diffusion. Thus, Brownian motion can't be the direct role in thermal conductivity enhancement. Wang [41]'s work also support this conclusion.

Because the interfacial atom structure around nanoparticles in nanofluids is more orderly arranged than base fluid, it would be expected to lead a higher thermal conductivity. However, it may not play the key role for such much enhancement.

In crystalline solids, for example the nanoparticle in bulk status, heat is carried by phonon. From the microscopic point of view, if the ballistic phonons initiated in one particle can persist in the liquid and reach a nearby particle, a major increase of thermal conductivity is expected. This is possible because Brownian motion makes particles closer.[41]

Clustering of particles can create paths of lower thermal resistance, thus the nanofluids have higher thermal performance than base liquids. This has been observed in literature.[35, 42] One thing needs to be care is that large clustering leads to sediment.

5.2 Introduce about azeotrope

Two concepts are interpreted. A zeotrope is a chemicals mixture when the composition of the vapor and the liquid phase at the vapor-liquid equilibrium state is never the same. Dew point and bubble point curve do not trouch each other over the entire composition range with the exception of the pure components (curve end points). [43]The fig. 5.1 shows the zeotrope mixture.

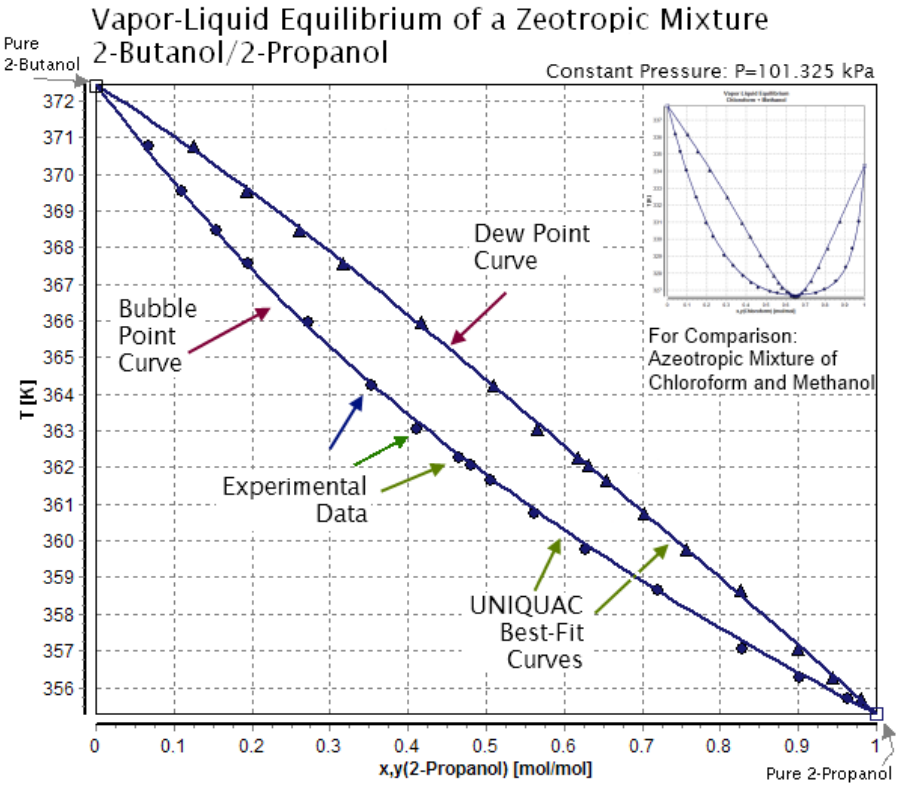

Figure 5.1 Vapor-liquid equilibrium of a zeotropic mixture

An azeotrope is a mixture of two or more liquids in such a way that components cannot be altered by simple distillation. It means that when boiling happens, the vapor has the same proportions of constituents as the unboiled mixture. Typical azeotropes of water are ethanol (95.5% by weight), n-propanol (71.7% by weight), sulfuric acid (98% by weight) and so on. Typical azeotropes of ethanol are benzene (67.6 by weight), ethyl acetate (69.2% by weight) and so on. [44, 45]In simple words, azeotrope has fixed boiling point.

In this thesis, ethanol-water azeotrope will be researched. Also, several fluids mixture combination will be studied experimentally.

5.3 Experiment procedure

Nanofluids can be produced by two techniques. One is single-step techniques. It means that simultaneously makes and disperses the nanoparticles into the base fluids. Another way is two-step technique. It disperses nanoparticles, which are prepared previously, into base fluid. Most open literatures, including this thesis, use this method to produce nanofluids for their research. The base fluid is methanol for our nanofluids experiment. The provider of aluminum oxide nanoparticles is US research Nanomaterials, Inc. Its purity is 99+% and average particle size is 20nm. Firstly, we disperse nanofluids into methanol and stir for 10 minutes. Then put the mixture into ultrasonic water bath for 2 hours. Fig 5.2 shows the nanofluids in flask.

Figure 5.2 Figure of Al_2O_3 methanol nanofluids

The same experiment system mentioned in chapter 4.2 is used.

5.4 Results and discussion

5.4.1 Nanofluids results

The following figure shows the nanofluids experiment results. Figure (a), (b), (c) and (d) are results for 25W, 100W, 200W and 300W respectively. it compares the fluids about pure methanol, 2.5% and 1%

volume fraction aluminum dioxide (Al_2O_3)-methanol nanofluids. All these are at the same initial filling, 0.2. To reduce the errors caused by environment, all experiments are conduced in one day and water jacket inlet temperature is kept constant.

The temperature shows the pipewall temperature in evaporator, in detail, 7th and 9th thermocouple, which is the same serial number as chapter 4.

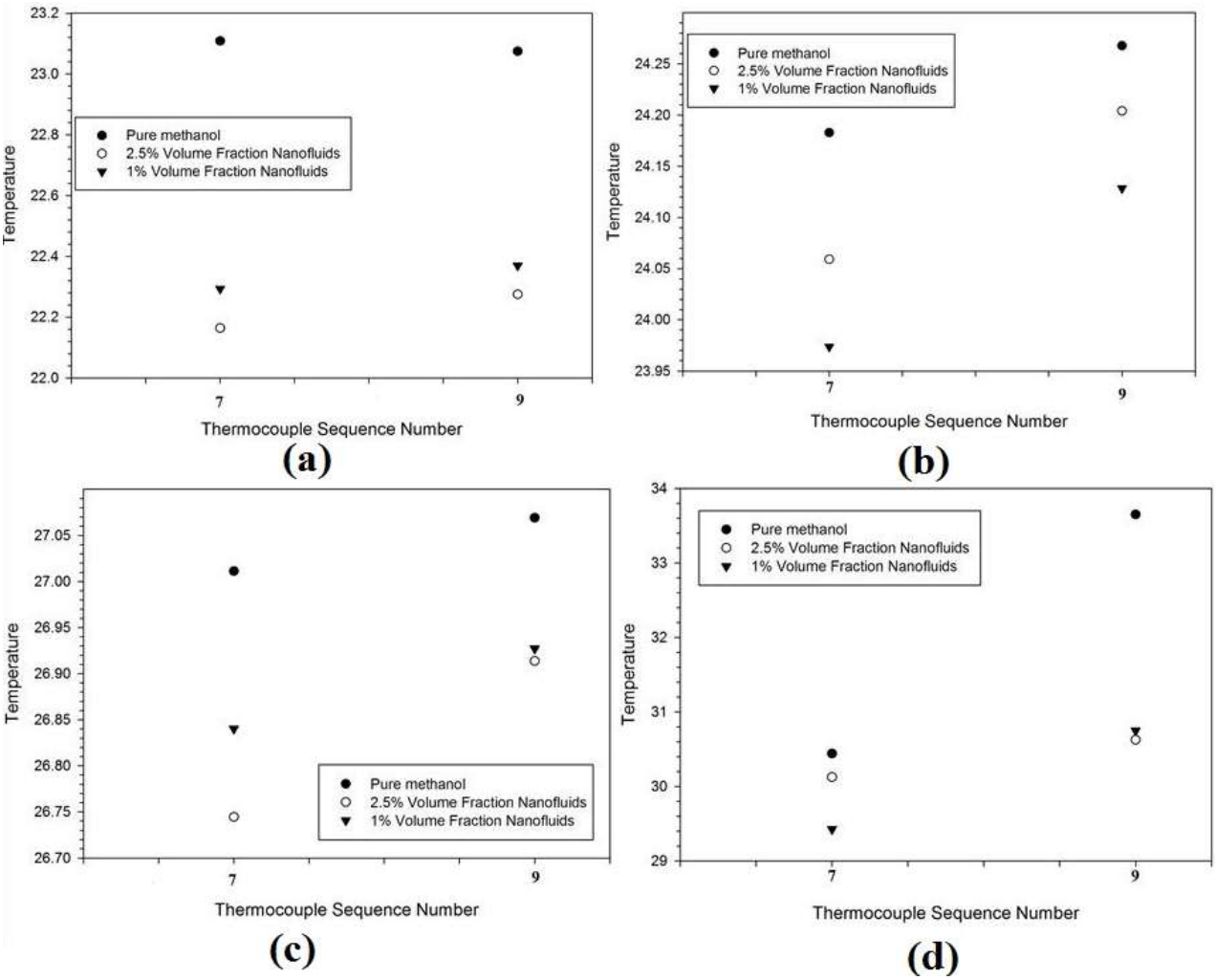

Figure 5.3 Nanofluids experiment results

The following figure show the experiment results from temperature different of view. The temperature difference is the one between vapor temperature and outer pipewall temperature. This is one of the most essential parameter determining the thermosyphon performance. The lower temperature difference indicates that the thermal resistance is lower. At the same temperature different from TPCT bottom to top, it can trafer more heat.

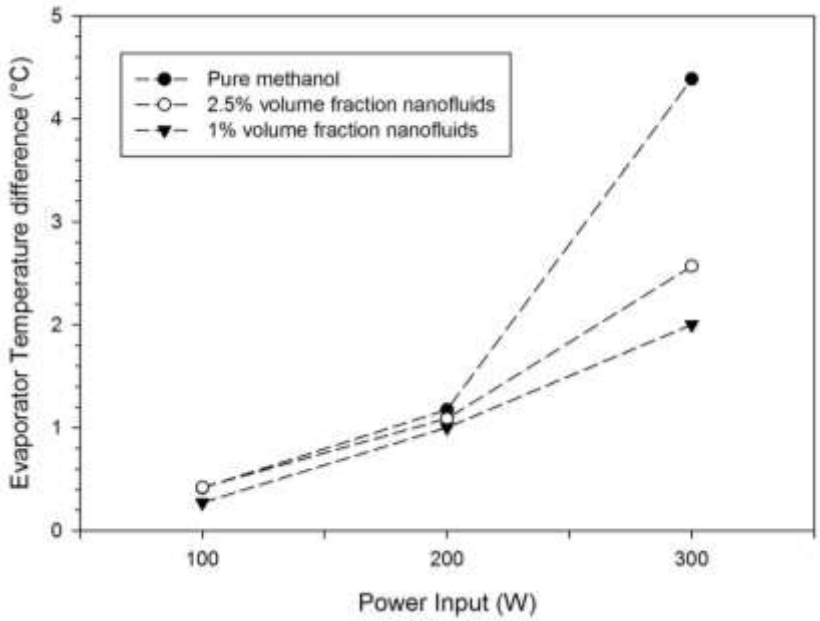

Figure 5.4 Temperature difference comparison for nanofluids

Based on the above two figures about nanofluids, the conclusion is made that nanofluids enhance the thermosyphon performance.

We expect larger volume fraction nanofluids could enhance more as referrences show larger one could enhance thermal conductivity more. However, our experiment did not show that. Viscousity, heat of vaporization and others are all possible reason for that.

5.4.2 Mixture results

The following figure shows the temperature distribution for methanol and ethanol mixture. Chapter 4 shows the distribution for methanol and ethanol respectively. Although they have different filling ratio, we still get some interesting findings. The first one is that the temperature distribution is not smooth. Theoretically, the temperature in evaporator film area is going down along pipewall because of the film sickness showing in fig. 2.7. Then goes up sharply because liquid pool has very low heat transfer coefficiency. This mixture is zeotrope, thus in the liquid film the components are not evenly distributed. Some unsteady area may occur. The second finding is that the pool temperature at 25W is around 3 °C higher than 100W and 200W power input. The third finding is that the performance of this mixture is worse than both pure methanol and pure ethanol.

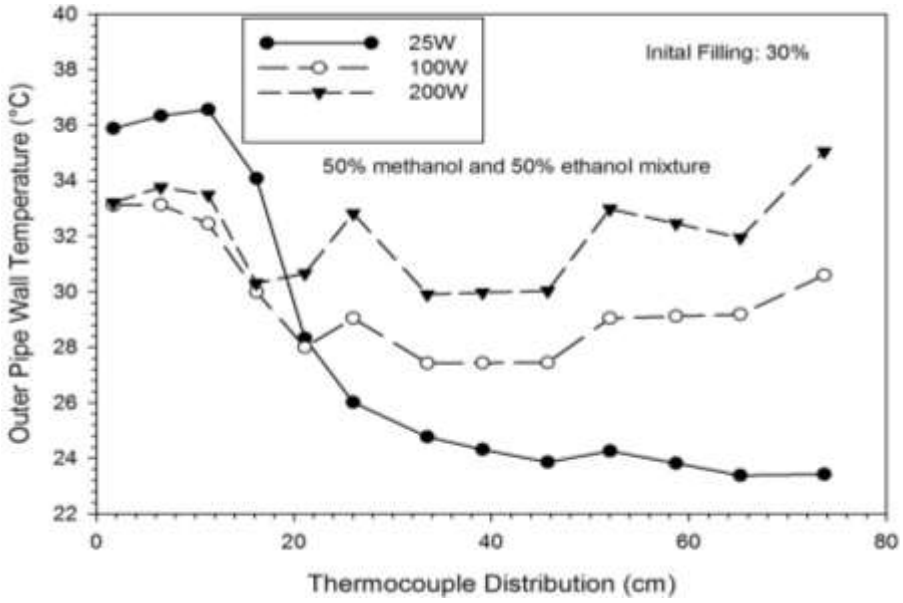

Figure 5.5 Figure of temperature distribution of methanol and ethanol mixture

The following chart shows the methanol proportion in vapor. It is calculated by Dalton's law. In half-half mixture, the vapor in operation is far from even.

Table 5.1 Chart of vapor proportion analysis

Power Input(W)	Vapor Temperature(°C)	Vapor Pressure (Pa)	Methanol Sat. P (Pa)	Ethanol Sat. P (Pa)	Methanol Proportion in Vapor
25	22.53	14700	14918	6885	0.97
100	24.73	14629	16736	7827	0.76
200	26.63	16048	18471	8730	0.75

5.4.3 Azeotrope results

The following figure shows the results from azeotrope. The ethanol proportion is 95.5% by weight and the initial filling for TPCT is 0.3.

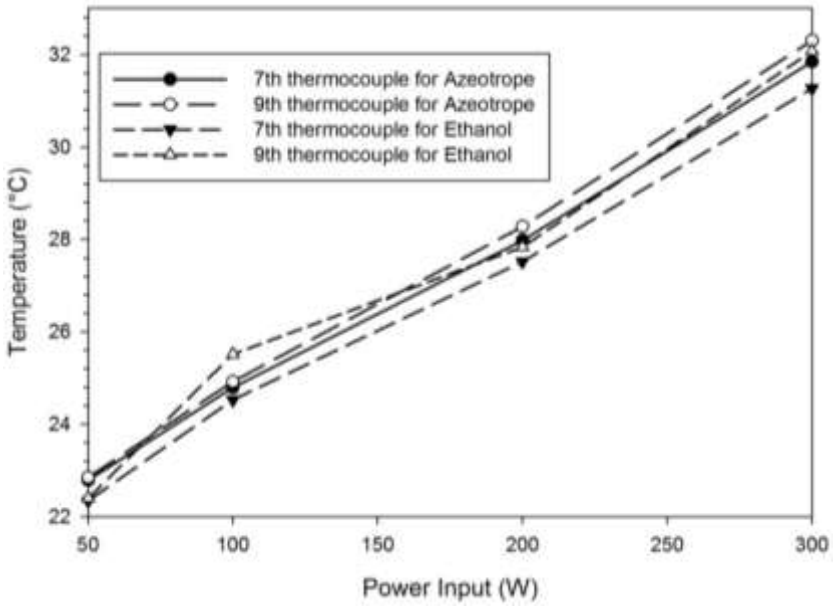

Figure 5.6 Figure of ethanol-water azeotrope

Conclusion

Firstly, detailed heat transfer mechanisms are discussed. Geometrically, it contains three parts, condenser, adiabatic section and evaporator, and each of them has three possible mechanism, natural convection, nucleate boiling and transit convection between these two. In evaporator, it has liquid film and liquid pool, more complex than condenser, which only contains liquid film. However, the liquid films in evaporator and condenser have distinct heat transfer mechanism. For all these mechanism, either analytical model or empirical equations are found.

A numerical model is built based on the literature reviews. It is suitable for any kind of liquids and covers wide range of geometry size and power input. Typically in this thesis, methanol ethanol and water results are listed. Geometry influence on thermosyphon performance, including condenser length, adiabatic section length, evaporator length and diameter are studied. It indicates that larger diameter, longer evaporator and condenser length could enhance performance a lot and adiabatic length has little effect.

An experiment system is built up. Through this, power input and working fluids filling ratio are controlled based on need. Temperature along outer pipe wall and vapor pressure are collected by this system. Comparison between simulation and experiment is conducted. In condenser part, experiment and simulation are within good agreement; in evaporator below 200W power input, it has good agreement, but for higher power input, the experiment results are larger than simulation results.

The data indicate that our experiment has relative high accuracy as vapor temperature and adiabatic temperature are less than 0.2 Celsius degree different. The experimental results from Ethanol (ranging from10% to 20% filling ratio) and Methanol (from 5% to 25% filling ratio), covering power throughout for 50W, 100W, 200W, 300W, shows that at the same power throughout, the vapor temperature is independent of initial filling ratio. Temperature distributions for both methanol (15% ratio) and ethanol (10% ratio) are listed. The experiment results demonstrate the analytical model. The data points in pool have relative high temperature because it is in low heat transfer efficiency area. In the film area, the top has higher temperature and then reduces gradually. This is caused by the film thickness variation as thicker film, the upper area, contributes more thermal resistance.

The operation limits are observed in our experiments. Thus, two conclusions are made: (a) at high power throughput condition, low initial filling could cause irregular high temperature distribution in liquid film area; (b) CCFL or LFDL is related to liquid type. For water, a interesting temperature recording is listed. Some references call it geyser phenomenon. I don't agree with it because this oscillation is observed in film area.

Creatively, new fluids are applied in this project. Experiment data about aluminum oxide nanofluids, ethanol-water azeotrope and ethanol-methanol mixture are listed. Seldom has any reference applied these working fluids. Ethanol-water azeotrope and ethanol-methanol mixture results is not all better than pure methanol. But these combinations expand the application field. For example, considering the healthy problem, ethanol azeotrope thermosyphon is applied instead of methanol. One important finding is that nanofluids thermosyphon has better performance than its base liquid thermosyphon.

Reference

[1] E. Hahne and U. Gross, "The influence of the inclination angle on the performance of a closed two-phase thermosyphon," *Journal of Heat Recovery Systems,* vol. 1, pp. 267-274, 1981.

[2] S. Noie, M. Sarmasti Emami, and M. Khoshnoodi, "Effect of inclination angle and filling ratio on thermal performance of a two-phase closed thermosyphon under normal operating conditions," *Heat transfer engineering,* vol. 28, pp. 365-371, 2007.

[3] P. Terdtoon, M. Shiraishi, and M. Murakami, "Effect of inclination angle on heat transfer characteristics of closed two-phase thermosyphon," in *Proc. 7th Int. Heat Pipe Conf*, 1990.

[4] K. Negishi and T. Sawada, "Heat transfer performance of an inclined two-phase closed thermosyphon," *International Journal of Heat and Mass Transfer,* vol. 26, pp. 1207-1213, 1983.

[5] U. Gross, "Reflux condensation heat transfer inside a closed thermosyphon," *International journal of heat and mass transfer,* vol. 35, pp. 279-294, 1992.

[6] H. Uehara, Kusuda, H., Nakaoka, T., Yamada, M.,, "Filmwise condensation for turbulent flow on a vertial plate," in *Heat Transfer-Japanese Research* vol. 12, 96 ed, 1983.

[7] U. Gross and E. Hahne, "Reflux condensation inside a two-phase thermosyphon at pressures up to the critical," in *Proceedings of the International Heat Transfer Conference, San Francisco*, 1986, pp. 1613-1620.

[8] M. Shiraishi, K. Kikuchi, and T. Yamanishi, "Investigation of heat transfer characteristics of a two-phase closed thermosyphon," *Journal of Heat Recovery Systems,* vol. 1, pp. 287-297, 1981.

[9] H. Jialun, M. Tongze, and Z. Zhengfang, "Investigation of boiling liquid pool height of a two-phase closed thermosyphon," in *Proceedings of the 8th International Heat Pipe Conference, Beijing*, 1992.

[10] H. Imura, H. Kusuda, J.-I. Ogata, T. Miyazaki, and N. Sakamoto, "Heat transfer in two-phase closed-type thermosyphons," *JSME Transactions,* vol. 45, pp. 712-722, 1979.

[11] M. Semena and Y. F. Kiselev, "Heat-exchange processes in the heat-supply zones of two-phase thermosiphons operating on freons 11, 113, and 142 and on water and ethanol," *Journal of Engineering Physics and Thermophysics,* vol. 35, pp. 895-899, 1978.

[12] S. S. Kutateladze, "Fluid Mechanics," *Soviet Researc,* 1972.

[13] U. GroB, "Pool Boiling Heat Transfer Inside a Two-Phase Thermosyphon-Correlation of Experimental Data," in *Proc. 9th Int. Heat Trans. Conf*, 1990, pp. 57-62.

[14] M. S. El-Genk and H. H. Saber, "Heat transfer correlations for small, uniformly heated liquid pools," *International journal of heat and mass transfer,* vol. 41, pp. 261-274, 1998.

[15] W. M. Rohsenow, "A method of correlating heat transfer data for surface boiling of liquids," Cambridge, Mass.: MIT Division of Industrial Cooporation,[1951]1951.

[16] T. UEDA, T. MIYASHITA, and P.-h. Chu, "Heat transport characteristics of a closed two-phase thermosyphon," *JSME international journal. Ser. 2, Fluids engineering, heat transfer, power, combustion, thermophysical properties,* vol. 32, pp. 239-246, 1989.

[17] F. Kaminaga, Y. Okamoto, T. Suzuki, and T. Ma, "Study on boiling heat transfer correlation in a closed two-phase thermosyphon," in *Proceedings of the 8th International Heat Pipe Conference, Beijing*, 1992.

[18] M. El-Genk and H. Saber, "Heat transfer correlations for liquid film in the evaporator of enclosed, gravity-assisted thermosyphons," *Journal of heat transfer,* vol. 120, pp. 477-484, 1998.

[19] M. S. El-Genk and H. H. Saber, "Flooding limit in closed, two-phase flow thermosyphons," *International journal of heat and mass transfer,* vol. 40, pp. 2147-2164, 1997.

[20] J. Reed and C. Tien, "Modeling of the two-phase closed thermosyphon," *ASME Transactions Journal of Heat Transfer,* vol. 109, pp. 722-730, 1987.
[21] B. Jiao, L. Qiu, X. Zhang, and Y. Zhang, "Investigation on the effect of filling ratio on the steady-state heat transfer performance of a vertical two-phase closed thermosyphon," *Applied Thermal Engineering,* vol. 28, pp. 1417-1426, 2008.
[22] T. Ueda, M. Inoue, and S. Nagatome, "Critical heat flux and droplet entrainment rate in boiling of falling liquid films," *International Journal of Heat and Mass Transfer,* vol. 24, pp. 1257-1266, 1981.
[23] K. Isao and I. Mamoru, "Drift flux model for large diameter pipe and new correlation for pool void fraction," *International journal of heat and mass transfer,* vol. 30, pp. 1927-1939, 1987.
[24] S. Chen, J. Reed, and C. Tien, "Reflux condensation in a two-phase closed thermosyphon," *International journal of heat and mass transfer,* vol. 27, pp. 1587-1594, 1984.
[25] H. Jouhara and A. J. Robinson, "Experimental investigation of small diameter two-phase closed thermosyphons charged with water, FC-84, FC-77 and FC-3283," *Applied thermal engineering,* vol. 30, pp. 201-211, 2010.
[26] A. Mills, "Basic Heat and Mass Transfer Prentice-Hall," *Upper Saddle River, NJ, USA,* 1999.
[27] S. Lee, S. U. Choi, S. Li, and, and J. Eastman, "Measuring thermal conductivity of fluids containing oxide nanoparticles," *Journal of Heat Transfer,* vol. 121, 1999.
[28] S. K. Das, N. Putra, P. Thiesen, and W. Roetzel, "Temperature dependence of thermal conductivity enhancement for nanofluids," *Journal of Heat Transfer,* vol. 125, p. 567, 2003.
[29] S. U. Choi, X. Xu, and X. Wang, "Thermal conductivity of nanoparticle-fluid mixture," *Journal of thermophysics and heat transfer,* vol. 13, 2012.
[30] H. Xie, J. Wang, T. Xi, Y. Liu, F. Ai, and Q. Wu, "Thermal conductivity enhancement of suspensions containing nanosized alumina particles," *Journal of Applied Physics,* vol. 91, pp. 4568-4572, 2002.
[31] D. Wen and Y. Ding, "Experimental investigation into convective heat transfer of nanofluids at the entrance region under laminar flow conditions," *International Journal of Heat and Mass Transfer,* vol. 47, pp. 5181-5188, 2004.
[32] H. Masuda, A. Ebata, K. Teramae, and N. Hishinuma, "Alteration of thermal conductivity and viscosity of liquid by dispersing ultra-fine particles," *Netsu Bussei,* vol. 7, pp. 227-233, 1993.
[33] C. H. Li and G. Peterson, "Experimental investigation of temperature and volume fraction variations on the effective thermal conductivity of nanoparticle suspensions (nanofluids)," *Journal of Applied Physics,* vol. 99, pp. 084314-084314-8, 2006.
[34] W. Yu, D. M. France, S. U. Choi, and J. L. Routbort, "Review and assessment of nanofluid technology for transportation and other applications," Argonne National Laboratory (ANL)2007.
[35] J. Eastman, S. Choi, S. Li, W. Yu, and L. Thompson, "Anomalously increased effective thermal conductivities of ethylene glycol-based nanofluids containing copper nanoparticles," *Applied Physics Letters,* vol. 78, pp. 718-720, 2001.
[36] K. Hong, T.-K. Hong, and H.-S. Yang, "Thermal conductivity of Fe nanofluids depending on the cluster size of nanoparticles," *Applied Physics Letters,* vol. 88, pp. 031901-031901-3, 2006.
[37] T.-K. Hong, H.-S. Yang, and C. Choi, "Study of the enhanced thermal conductivity of Fe nanofluids," *Journal of Applied Physics,* vol. 97, pp. 064311-064311-4, 2005.
[38] Y. Ding, H. Alias, D. Wen, and R. A. Williams, "Heat transfer of aqueous suspensions of carbon nanotubes (CNT nanofluids)," *International Journal of Heat and Mass Transfer,* vol. 49, pp. 240-250, 2006.
[39] S. Murshed, K. Leong, and C. Yang, "Enhanced thermal conductivity of TiO< sub> 2</sub>— water based nanofluids," *International Journal of Thermal Sciences,* vol. 44, pp. 367-373, 2005.

[40] P. Keblinski, S. Phillpot, S. Choi, and J. Eastman, "Mechanisms of heat flow in suspensions of nano-sized particles (nanofluids)," *International Journal of Heat and Mass Transfer,* vol. 45, pp. 855-863, 2002.
[41] X. X. Xinwei Wang, and Stephen U. S. Choi., "Thermal Conductivity of Nanoparticle - Fluid Mixture," *Journal of Thermophysics and Heat Transfer,* vol. 13, pp. 474-480, 1999.
[42] J. Eastman, U. Choi, S. Li, G. Soyez, L. Thompson, and R. DiMelfi, "Novel thermal properties of nanostructured materials," *Journal of Metastable and Nanocrystalline Materials,* vol. 2, pp. 629-634, 1999.
[43] W. J. Tamir A., "Vapor-Liquid Equilibria of Isobutanol-n-Butanol and Isopropanol-sec-Butanol Systems," *J.Chem.Eng.Data, 20(4),* pp. 391-392, 1975.
[44] CRC, *Handbook of Chemistry and Physics,44th ed,* pp. 2143-2184.
[45] *Lange's Handbook of Chemistry, 10th ed,* pp. 1496-1505.